Chapter 1

INTRODUCTION

1.1 Background

At present, about two-third of the power generation is based on thermal units comprising of steam and gas turbines, rest based on hydro and nuclear and other non-conventional systems. Except direct energy systems where one form of energy is directly converted into electricity, entire power is generated through the turbine used as a prime mover. Thus, the efficiency of power plant is greatly depends on the performance of turbines. Average life of a thermal power plant is about 30 years. Cost of installing new capacity is much more than the capacity obtained by improving the performance of existing units. New blades have very smooth surface finish and fine profile, but as the turbine operates under severe conditions of temperature and pressure, with usage the blade surface deteriorates under the combined effect of corrosion, erosion and deposits. In the steam turbines, the steam flows between the blade passages of fixed and moving blades and due to the movement of the fluid, there is constant wear of the blade surfaces. Some solid particles come along with the steam and hit the blade surfaces. Also, there are salts dissolved in steam that get precipitated and deposited over the blades. In some cases erosion is more dominated while in other cases corrosion or deposits are more significant, depending on the conditions prevailing in the turbine. These factors adversely affect the blade surface, leading to increase in roughness. All these badly affect the blade profile of the turbine which gets distorted. Similar effects are also seen in hydro turbines, where erosion is caused due to impact of silt coming with the water. In case of gas turbine, in spite of efficient functioning of air filters, the dust particles enter into compressor and turbine and erode the blades.

1.2 Surface roughness

Surface roughness, often shortened to roughness, is a measure of the texture of a surface. It is quantified by the vertical deviations of a real surface from its ideal form. If these deviations are large, the surface is rough; if they are small the surface is smooth.

Roughness is typically considered to be the high frequency, short wavelength component of a measured surface

Roughness plays an important role in determining how a real object will interact with its environment. Rough surfaces usually wear more quickly and have higher friction coefficients than smooth surfaces. Roughness is often a good predictor of the performance of a mechanical component, since irregularities in the surface may form nucleation sites for cracks or corrosion. Although roughness is usually undesirable, it is difficult and expensive to control in manufacturing. Decreasing the roughness of a surface will usually increase exponentially its manufacturing costs. This often results in a trade-off between the manufacturing cost of a component and its performance in application.

1.3 Existence of surface roughness – why

On any finished surface, imperfections are bound to be there and these take the form of a succession of hills and valleys which vary both in height and in spacing and result in a kind of texture which in appearance or feel is often characteristic of the machining process and its accompanying defects. The several kinds of departures are there on the surface and these are due to various causes. Roughness or texture in the form of a succession of minute irregularities is produced directly by the finishing process employed e.g. while using a single point tool. The characteristic roughness produced by the tool is not the only cause of roughness in case of machining operations, but the more openly spaced component or roughness are also produced from faults in the machining operation. Moreover the type of operation performed by any device and the environment in which that device is being operated is also contributed towards roughness. In practice the complete roughness commonly represents a combination of irregularities of various kinds and magnitudes arising from several different causes and the individual effects of the separate contributing factors can't always be readily distinguished.

Thus for the complete study of the surface roughness, it is essential that the measurement and analysis of all the component elements and an assessment of the effects of the resulting combined texture be made. All this being very difficult and tedious job, in practice all that is essential is that a practical method of assessment be followed, the result of which can be readily compared with a specified requirement of quality,

preferably on the numerical basis. It is done by analyzing the form of profile revealed by a plane section through the surface. The measurement of surface roughness poses a problem in three dimensional geometry, but for simplification purposes, it is better to reduce it into two dimensional geometry by confining individual measurement to the profiles of plane sections taken through the surface. The direction of measurement is usually perpendicular to the direction of the predominant surface markings. The shape of the hills and valleys which constitute surface roughness is best studied in a cross-section normal to the surface using a stylus instrument which plots a graph in which the minute irregularities of the surface are magnified to 50,000 times or even greater, whereas the length over which observations are made is magnified only by 50 to 300 times. Thus the above graph does not give a real representation of the surface nature, but a distorted view, but it gives very useful information. From this curve the height of the irregularities (total or average value), separation of the crests (separation) can be easily noted. When the irregularities are comparatively uniform in shape and size, then the distance between the successive peaks is described as pitch or dominant spacing. It may be appreciated here that the surface roughness is concerned both with the size and the shape of the irregularities e.g., in certain profile the height of departure from the nominal profile may be same but the spacing of the irregularities may be wider or closer, or the space of the irregularities may be of various forms. Thus realizing that both size and shape (i.e. height of irregularities, their spacing and form) are important for specifying surface roughness, it is not considered possible to express the complete roughness characteristics by means of any single number. The normal practice is, therefore, to specify Ra (roughness) value to define the quality or grade, and the manufacturing process which serves to produce the type of roughness.

1.4 Motivation

The deterioration of the surface finish has direct effect on the efficiency of the turbine, leading to increase in losses. Turbine blade roughness is one of the major contributors to losses, this has been confirmed from steam path audits conducted at Vindhyachal, Ramagundam and many others power stations of National Thermal Power Corporation Limited.

1.5 Problem Statement

The primary objective of this project is to numerically study the effect of change in blade profile due to roughness on the turbine efficiency. On the model of rectilinear cascade of turbine blades, discretization will be done with the help of Gambit®, with various grades of roughness at different positions. Then Fluent® is used on the flow through the blades. From the data, effect of roughness on mass average loss coefficient, total and static pressure coefficient, turbulence kinetic energy, turbulence intensity, Mach number will be studied.

1.6 Expected outcome and actual achieved

By determining the effect of roughness on the efficiency of the steam and gas turbines, various decisions regarding the replacement of the blades can be taken with improved certainty. Based on this information a cleaning schedule can be made and updated regularly and methods can be developed for improving surface finish. Losses occurring due to change in blade profile and due to increase in roughness can also be ascertained

1.7 Effect of roughness over performance

The roughness created over the blade surface either on rotor or stator blade affects adversely on performance of the turbine. The roughness created by the machining process may be uniform all over the blade whereas the roughness created by erosion, corrosion and deposition may be at different localized places. Roughness created by erosion make the blade thinner and deposition make the blade thicker in addition to the roughness.

Due to the change in profile and roughness, the performance of the turbine has been studied computationally in this thesis. The basic concepts about the turbo machines is presented in chapter 2 and detail of work carried out by different researches have been presented in chapter 3. Chapter 4 covers the description of cascade modeling on fluent software. The results and discussion have been presented in chapter 5 followed by conclusions in chapter 6. The future scope of work, references, appendix containing the coordinates of the profiles and geometries of the cascades are given at the end.

Chapter 2

LITERATURE REVIEW (Basic concepts)

An important class of fluid machine has, as its characteristic, the transfer of energy between a continuous stream of fluid and an element rotating about fixed axis. Such a machine is classed as a turbo machine: fans, pumps, compressors and turbines come into this group. Discussion is limited in this book to those machines where the fluid is at all times totally enclosed by the machine elements, so that it is controlled by passage walls. This restriction excludes the Pelton turbine and wind turbines. The machines will be categorized by flow path and by function, as the typical machines to be covered. The ideal performance laws are introduced first: the discussion centres on the Euler equation and its applications, it being assumed that basic fluid mechanics and the principles of vector diagrams are understood. The incompressible cases are treated first, and then attention is paid to the problems posed by compressible considerations. Shock wave theory and basic gas dynamics are also taken to be understood by the reader.

2.1 Linear turbine cascade

A row of blades representing the blade ring of an actual turbo machine is called cascade grid, lattice or a mesh of blades. In a straight or “rectilinear cascade” the blade are arranged in a straight line. The blades can also in an annulus, thus representing an actual blade row. This arrangement is known as an “annular cascade”.

The linear turbine cascade there exists a relative motion between the blade tip surface and the casing wall. As shown in Fig, 2.1 the cascade wind tunnel has an open-circuit type wind tunnel, an inlet duct, a linear turbine cascade, and an exit duct in turn. The flow coming out from the wind tunnel develops to a turbulent boundary layer flow over the top and bottom walls of the inlet duct, after passing a trip wire and a sand paper. The inlet duct has a cross section of 0.42 m _ 0.32 m. The turbine cascade has six large-scale linear turbine blades, and the entrance of its central flow passage is located about 1.2 m downstream of the wind tunnel exit. The exit duct has a tailboard to adjust periodicity among the blade passage flows. The six large-scale turbine blades are fabricated based on the profile of a first-stage turbine rotor blade for power generation, and they are made of

aluminium. The chord length, c, axial chord, b, pitch, p, and span, s, of the large-scale blade. are 217.8 mm, 196.0 mm, 151.6 mm, and 320.0 mm, respectively. The span is determined on the basis of an aspect ratio of the original blade (s/c = 1.47). The blade inlet and outlet angles defined are b1 = 56.4^{o} and b2 = 62.6 ^{o}, respectively. Thus the blade has a turning angle of 119 ^{o}. The blade profile used in this study.

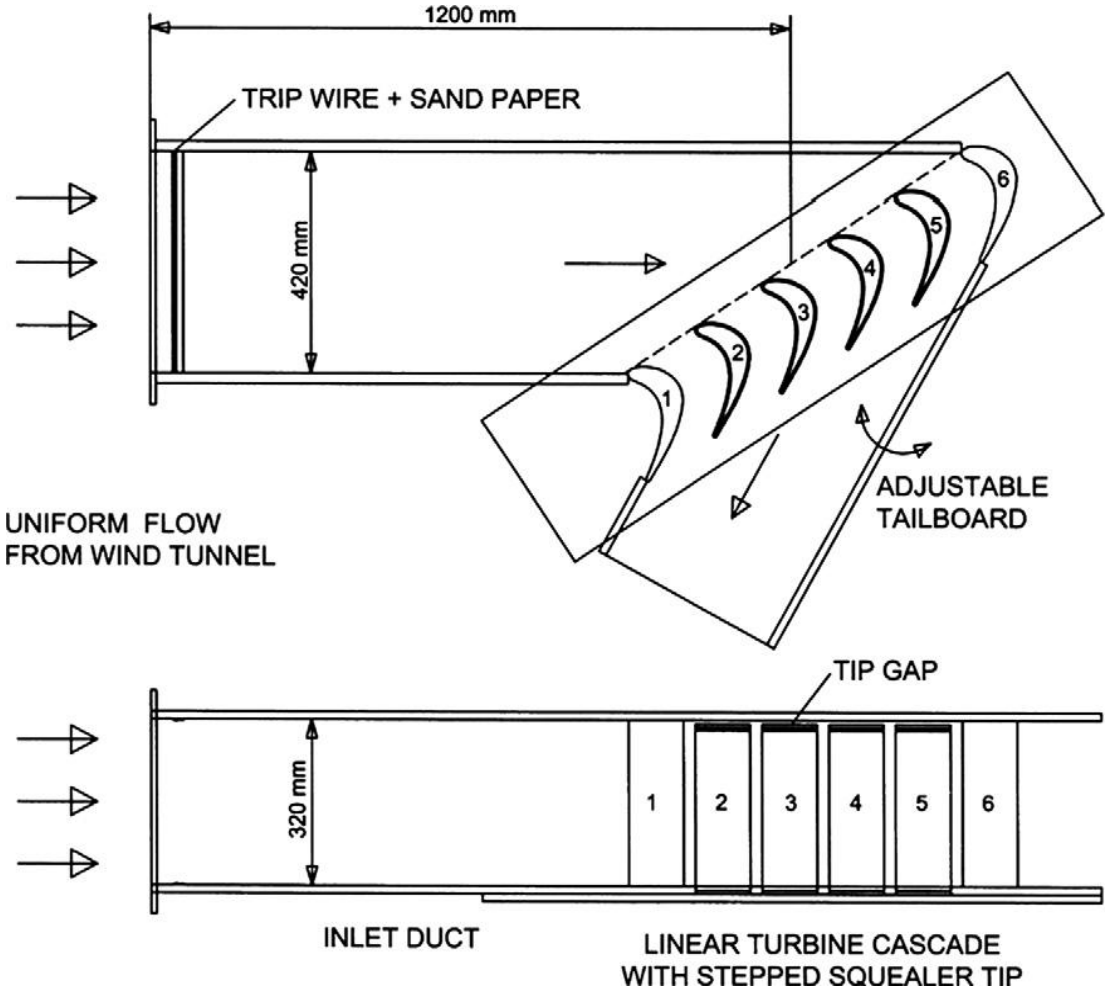

Figure 2.1Turbine cascade wind tunnel

2.2 Basic Turbine blade concept

The cross section of a turbine blade with disk the blade is mounted the disk at its hub. The disk is located as the gas turbine shaft. High temperature and high pressure flow originally coming from the combustor rotates the turbine blades.

The basic turbine cascade terminology is shows figure.2.2 The cross section of the succeeding blade row of rotor and stator creates the turbine flow enter the cascade through the leading edge of the blade and leaves it through the trailing edge the spacing between the blades is called as pitch. Blade inlet and exit angles as well as flow inlet and exit angles are also shown in figure.2.2.

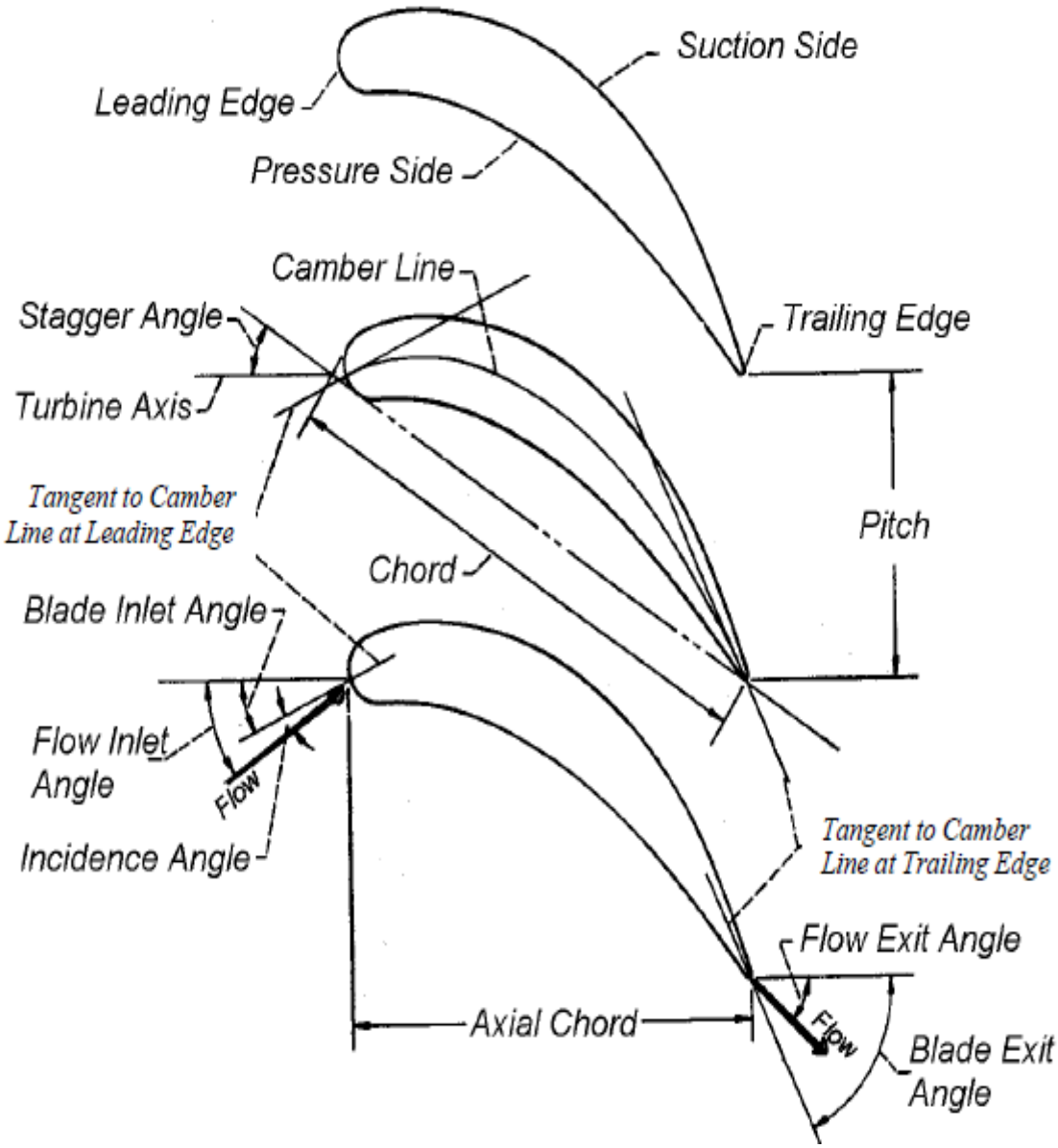

Figure:2.2 Turbine Cascade Terminology

2.3 Coordinate system

An illustration of air flowing through a turbine stage in given the coordinate system consists of three directions.

Axial direction – parallel to the axis of location.

Radial direction – Radial through the axis of rotation.

Tangential direction – Tangent to the rotating stage.

For Analysis of flow in the radial axial plane depicts the circumferentially averaged (blade to blade average) calculations we can ignore blade to blade variation of parameter values and just use average values. Such a calculation is called axis symmetric or through flow analysis.

Calculation made in the axial tangential or radial tangential planes are usually at same constant value (rather than for average conditions) of the third coordinate. Velocity diagram as well as blade to blade velocity variation calculations are usually made in these planes. When flow is predominantly radial such as at the inlet to a radial flow turbine, the radial tangential plane is used. When flow is predominantly axial, such as in an axial flow turbine, the axial tangential plane is used.

2.4 Energy Transfer

The energy transfer relation for any turbo machine is related to mass momentum and energy conservation as applied to a fluid traversing a rotor. Fluid enters the rotor at point 1 passes through the rotor and leaves at point 2 the directions and radius are arbitrary periodic (steady) state condition is assumed with in the blade passage Further the velocity vectors at the inlet and exit are regarded as representing the average values for the mass flow being considered the magnitude change of axial velocity components corresponds to a change in axial force which is taken by a thrust bearing. The change in magnitude and radius of the tangential components of velocity corresponds to a change in angular momentum of the fluid and results in the desired tangential force F, net rotor torque is equal to the difference between the inlet and outlet of the products of tangential force F times radius r

Newton's 2^{nd} law of motion for a given mass in velocity V and time t is given as.

$$F = M\, dv/dt$$

In the tangential direction integrating from v =0 at t =0 to v =v at t = t and setting mass flow rate M =m/t yields.

$$F = mv$$

2.5 Blade loading

It is the change in tangential momentum of the fluid that results in the transfer of energy from the fluid to the rotor As the fluid flows through the cascade between each pair of blades. Through a curved passage a centrifugal force acts on it in the direction of the pressure (concave) surface. To counter balance a pressure force is established to turn the fluid through its curved path. The pressure force is directed normal to the flow and toward the suction (convex) surface. Thus the pressure in the passage is highest at the pressure surface and lowest at the suction surface. The resulting distribution of static pressure on the blade surfaces is illustrated where pressure is plotted against axial distance. At or near the blade loading edge there is a stagnation point where the velocity becomes zero and the pressure reaches its stagnation value. Figure 2.3

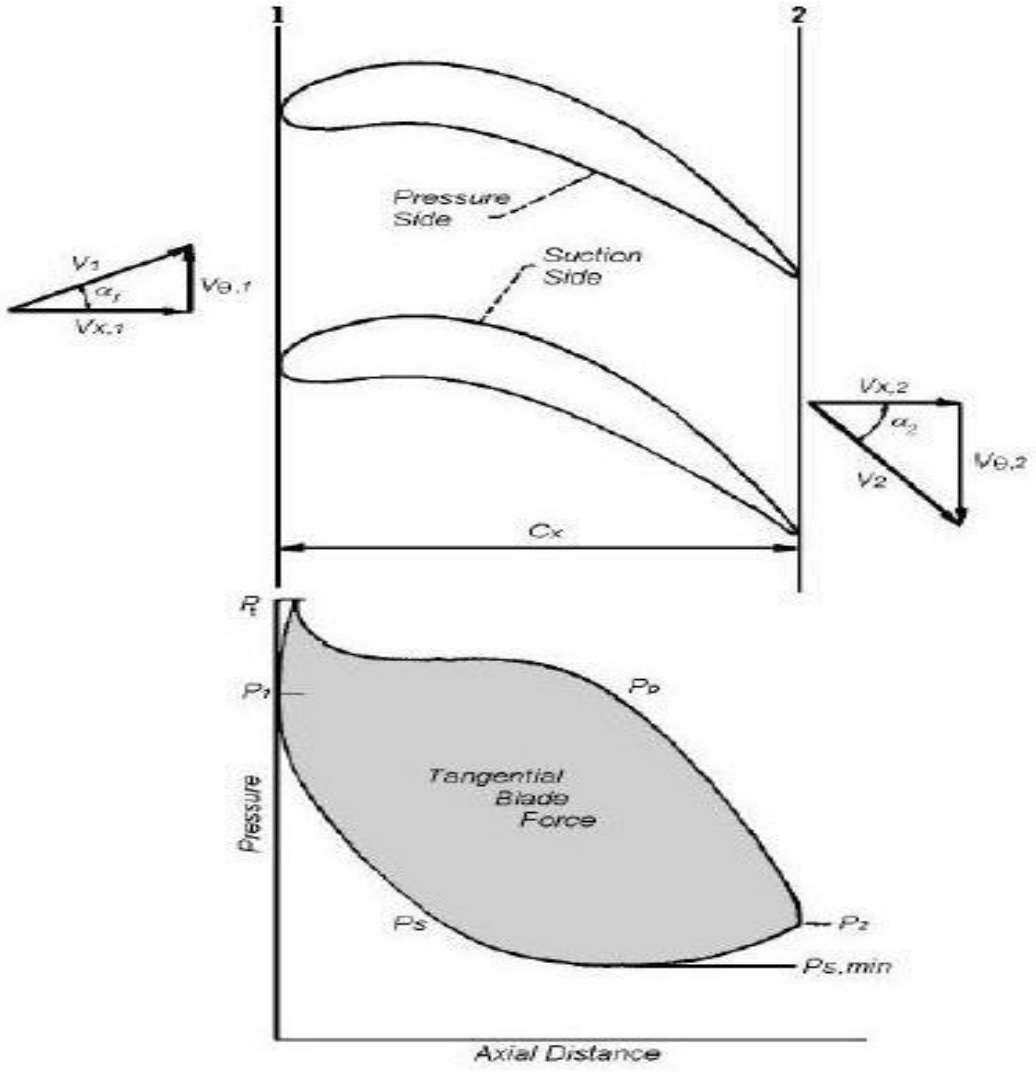

Figure:2.3 Cascade Velocity diagram & Surface Static pressure distribution.

The stagnation point is dividing point for the fluid flowing around the two sides of the blade. Starting from the stagnation point. The static pressure will often decrease below the exit. Pressure and then increase back up to the exit pressure. The pressure distribution curve illustrated in figure2.3 is called the blade loading diagram. The area between the curves represents the blade force acting in the tangential direction. Similarly static pressure on pressure surface, decreases from stagnation pressure at inlet till certain distance and remain same, and then decrease, sharply to each pressure.

2.6 Blade Forces

By definition the drag force is parallel to the direction of the mean velocity C_m and the lift normal . the resultant of lift and drag is the force F_r. This has another set of component F_x and Fy in the axial and tangential directions respectively. The aim of turbine designer is to obtain the maximum value of the tangential force on the cascade with a minimum value of the axial thrust (F_x) and pressure loss Δp_o.

It may be noted that, in a turbine, the forces are exerted by the fluid on the blade. The blade in turn exerts the same magnitude of forces in the opposite directions.

The entire cascade can be divided by the control surfaces surrounding each blade analysis of forces exerted on a blade can then be done by considering the flow through the control surface containing this blade.

Various relations can be written for the unit height of the blade. For simplicity, the axial velocity component and density of air are assumed to be constant across the control surface.

The continuity equation for the control surface gives

$$\dot{m} = \rho_1 c_{x1} (s \times 1) = \rho_2 c_{x2} (s \times 1)$$

But $\rho_1 \approx \rho_2 \approx \rho$

$$c_{x1} = c_{x2} = c_{xm}$$

Therefore $\dot{m} = \rho s c_{xm}$

2.6.1 Tangential force

The tangential force on the blade is equal to the rate of change of momentum in the tangential direction.

$$F_y = \dot{m} \{c_{y2} - (-c_{y1})\}$$

$$F_Y = \rho s c_{xm} (c_{y1} + c_{y2})$$

From velocity triangles

$$F_y = \rho s c^2_{xm} (\tan \alpha_1 + \tan \alpha_2)$$

Using exit and mean velocity triangles, the following relations are obtained.

F_y = (1/2 ρlc^2_{xm}) 2 (s/l) (tan α_1 + tan α_2)

This can be expressed in the form of dimensionless tangential force coefficients.

$$C_{Fy} = F_y / ½ \rho l c^2_{xm} = 2(s/l) (\tan \alpha_1 + \tan \alpha_2)$$

$$F_y = (1/2 \rho l c_2^2) 2 (s/l) \cos^2 \alpha_2 (\tan \alpha_1 + \tan \alpha_2)$$

$$C'_{fy} = F_y / ½ \rho l c_2^2 = 2 (s/l) \cos^2 \alpha_2 (\tan \alpha_1 + \tan \alpha_2)$$

2.6.2 Axial force

Generally, there is a static pressure drop across a turbine cascade. Therefore, the axial thrust is due to both the pressure difference and change of momentum in the axial direction.

$$F_x = (p_1 - p_2) s \times 1 + \rho (s \times 1) c_{xm} (c_{x1} - c_{x2})$$

For incompressible flow,

$$p_1 = p_{o1} - ½ \rho c_1^2$$

$$p_2 = p_{o2} - ½ \rho c_2^2$$

$$p_1 - p_2 = ½ \rho (c_2^2 - c_1^2) + (p_{o1} - p_{o2})$$

Substituting this in the expression for F_x, and assuming $c_{x1} = c_{x2}$

$$F_x = ½ \rho s (c^2_2 - c^2_1) + s\Delta p_o$$

From the velocity triangles at the entry and exit

$$c^2_2 - c^2_1 = c^2_{x2} + c^2_{y2} - c^2_{x1} - c^2_{y1} = c^2_{y2} - c^2_{y1}$$

$$F_x = ½ \rho s (c^2_{y2} - c^2_{y1}) + s\Delta p_o$$

$$F_x = ½ \rho s c^2_{xm} (\tan^2 \alpha_2 - \tan^2 \alpha_1) + s\Delta p_o$$

$$F_x = \rho s c^2_{xm} ½ (\tan \alpha_2 - \tan \alpha_1) (\tan \alpha_2 + \tan) + s\Delta p_o$$

But $½ (\tan \alpha_2 - \tan \alpha_1) = \tan \alpha_m$, therefore

$$F_x = ½ \rho s c^2_{xm} \tan \alpha_m (\tan \alpha_2 + \tan \alpha_1) + s\Delta \rho_o$$

Equation can also be written as

$$F_x = (1/2 \rho l c_2^2) (s/l) \cos^2 \alpha_2 (\tan^2 \alpha_2 - \tan^2 \alpha_1) + s\Delta \rho_o$$

In the dimensionless from

$$C_{Fx} = F_x / ½ \rho l c_2^2 = s/l \cos^2 \alpha_2 (\tan^2 \alpha_2 - \tan^2 \alpha_1) + s\Delta \rho_o / ½ \rho l c_2^2$$

The pressure loss coefficient for the cascade is defiend as

$$Y = \Delta \rho_o / ½ \rho l c_2^2$$

Therefore, the axial thrust coefficient is

$$C_{Fx} = s/l \cos^2 \alpha_2 \ (\tan^2 \alpha_2 - \tan^2 \alpha_1) = s/l \ Y$$

2.7 Zweifel's Criterion

Zweifel's defines a tangential force coefficient on the basis of a maximum hypothetical value.

It is assumed that a maximum tangential force on the blade is exerted in a reversible flow

($\Delta p_o = 0$) when the pressure and suction surfaces of the blade experience uniform static pressures of p_{o1} and p_{o2} respectively.

$$F_{ymax} = (p_{o1} - p_2)$$

For reversible flow,

$$p_{o1} - p_2 = p_{o2} - p_2 = \tfrac{1}{2} \rho c^2_2; \text{ therefore}$$

$$F_{ymax} = \tfrac{1}{2} \rho b c^2_2$$

Equations

$$C_Z = F_y / F_{ymax} = 2 (s/b) \ c^2_{xm} / c^2_2 \ (\tan \alpha_1 + \tan \alpha_2)$$

For constant axial velocity

$$C^2_{xm} / C^2_2 = C^2_{x2} / C^2_2 = \cos^2 \alpha_2$$

Therefore,

$$C_Z = 2 (s/b) \cos^2 \alpha_2 (\tan \alpha_1 + \tan \alpha_2)$$

For small blade chords, the values of the axial and actual chords are almost the same ($b \approx l$). For this condition Esq. a identical.

$$C_Z \approx C_{FY}$$

On the basis of cascade tests, zweifel recommends that the coefficient approximately 0.80. The criterion has been used to obtain the optimum pitch- chord ratio in turbine blade row.

2.8 Effect of inlet and exit velocities

Figure 2.3 shows a typical set of blade inlet and exit diagram as well as the static pressure distribution around a blade. The velocities shown are absolute velocity the blade design

under discussion here pertains to both rotor blade row as well as stator blade row. When referring to a rotor relative velocities are used . and for stator blade absolute are used in the equation and figure for sign convention the exit tangential velocity component and flow angle are taken as negative values.

2.9 Terminology used in cascade Analysis

Aspect ratio

Ratio of blade height to chord. If aspect ratio is reduced the contribution of secondary losses in total losses increases.

Blade angle

Included angle between tangents drawn on the camber line at leading edge and trailing edge with the axial or tangential direction are the blade angles at inlet and exit, respectively.

Camber angle

The angle between tangent drawn on the camber line at leading edge and chord line at inlet, the angle between tangent drawn on the camber line at trailing edge and chord line is camber angle at exit. The sum of camber angle at inlet and exit is camber angle.

Camber line

A blade section of infinitesimal thickness is a curved line known as camber line. This forms the backbone line of a blade of finite thickness.

Cascade

An infinite row of equidistant similar blade is called a cascade. When blades are arranged in a straight line the cascade is called rectilinear cascade. In annular cascades, the blades are arranged in an annulus. In a radial cascade the blades are arranged radial inward or outward direction.

Centerline average (c.l.a) or Arithmetic average (a.a) or Roughness height (R_{t})

This is the arithmetic average of the departure of the profile above and below its centerline, throughout the prescribed sampling length and in a plane substantially normal to the surface. It is therefore the ratio of sum of the area above the centerline and area below the centerline to total sampling length.

Chord

A straight line joining center of leading edge and center of trailing edge. The length of this line is blade chord.

Deviation

The difference between flow angle and blade angle at outlet is called deviation angle. It also may be positive or negative.

Flow inlet angle

Angle that the flow makes at inlet with the axial or tangential direction.

Flow outlet angle

Angle that the flow makes at outlet with the axial or tangential direction. It depends on pitch-chord ratio and stagger angle.

Incidence angle

The difference between flow angle and blade angle at inlet. It may be positive or negative.

Leading edge thickness

Edge of Blade where the flow enters.

Peak to valley height (R_p)

It is the difference between the mean heights of the peaks and valley.

Pitch-cord ratio

Ratio of pitch to the chord of the blade

Pressure and suction surface

The concave surface of the blade is called pressure surface, and convex surface is called suction surface.

Root mean square value (R_s)

Root mean square value is the square root of ratio of integration of square of distance *(y),* departure of the profile above and below its centerline with distance over the sample length to the sample length.

Sand roughness height (k_s)

Roughness formed by sand grain of size k_s when they are closely packed.

Span

Height of the blade from hub to tip.

Stagger angle

Stagger angle is the inclination of chord line with the axial or tangential direction. The shape of the channel changes with change in stagger angle, which results in change in pressure distribution and boundary layer thickness and hence losses. Increase in stagger angle (axial) increases semi-vane-less region and reduces the throat. For the same stagger angle, exit angle changes with pitch-chord ratio and for same pitch-chord ratio exit angle increase with increase in stagger angle.

Trailing edge thickness

The edge of the blade at flow exit end.

Tip gap height

The tip clearance gap between the stationary casing wall and the tip surface of a rotating turbine blade. Due to the presence of the pressure difference between the pressure and suction sides of the blade, flow leakages from the gap. It should be lowest possible.

Tip leakage

The tip leakage flow from the pressure side to the suction side is inevitably existent through the tip gap. This leakage flow develops into a tip leakage vortex near the blade suction surface, due to the interaction with the blade passage flow.

2.10 Roughness characterization

To analyze the effect of different level of roughness over the performance parameters, quantification of roughness is required .The roughness has been characterized on the basis of the height of peaks , the structure of roughness and the waviness of surface. The various terms employed for surface roughness are shown in figure.3.3 Sand roughness height (Ks) is the roughness formed by sand grain of size Ks when they are closely packed. Centreline averaged (c.l.a) or Arithmetic average (a.a) or Roughness height (Rt) is the arithmetic average of the departure of the profile above and below its centreline, throughout the prescribed sampling length and in a plane normal to the surface. It is therefore the ratio of sum of the area above and below the centreline to total sampling length. Peak to valley height (Rp) is the difference between the mean heights of the peak and valley. Root mean square value (Rs) is the square root of ratio of integration of square of distance (y), above and below its centreline with distance over the sample length to the sample length.

2.11 Roughness pattern

Discussed above erosion, corrosion and deposition depends on various factors and hence the roughness varies from hub to tip, leading edge to trailing edge and initial stage to last stage. The pattern of roughness observed by different authors is summarized here. Cotton and Schofield [1971] observed copper salts deposits of different levels of roughness in rotor and nozzle blades. Similarly, Boics and sari[1988] observed that deposits mainly on the pressure surface, Taylor [1990] observed that the first stage blades of TF-100 aircraft

turbine were the roughest (10.7 μm) on suction surface at leading edge region, whereas the same stage blades of TF-39 were roughest on pressure surface near mid chord (6.86μm) and trailing edge region (5.5 μm). Bons et al. [2001] observed that some region on both the suction and pressure surface are prone to specific roughness mechanism, and transition between rough and smooth regions are gradual but could be very abrupt.

In a 210 MW steam turbine, Samsher et. al [2006] observed that the rotor blades of initial stages of IP turbine are subjected to solid particle erosion at suction surface, and deposition over the pressure surface. The inlet steam in these turbines is superheated and the roughness can be attributed primarily to solid particle impact and deposits. The similar roughness was also observed in the rotor and stator blades of the initial stages of the LP turbine. The observations on the last four (5^{th} – 8^{th}) stages of LPT stator, i.e. roughness due to deposition only. The roughness's are predominantly in the form of bands (at mid-chord, leading edge) spread all over the span.

The magnitude and the statistical character of the roughness varied substantially from point to point around the blade, the blade thus does not have a single roughness value.

2.12 FLUID DYNAMICS OF FLOW OVER BLADES

2.12.1 Boundary layer growth over blade surface

As the flow moves over the surface, the boundary layer thickness growth with distance (X) in direction of flow (equation 1), the rate of growth also depends on pressure gradient,[Schlichting, 1968]

$$\delta_{99}/l = 5\sqrt{(x/Re)} \qquad (1)$$

(where δ_{99} is boundary layer thickness, l, characteristic length, Re Reynolds number)

The boundary layer in laminar for a small characteristic length (l), but for longer characteristic length, it becomes thicker, and after some length the flow inside it becomes unstable (transition) followed by increase in growth rate of the boundary layer thickness leading to turbulent Boundary layer. In presence of adverse pressure gradient, the boundary layer separates from the surface. Separation of boundary layer results in high loss of energy in the form of eddies.

Bammert and Sandsted [1980] observed that boundary layer thickness on the suction side for a smooth surface increases gradually up to 33% of contour length and then the rate of increase is more towards trailing edge with possibility of flow separation. On the

pressure side, the boundary layer thickness first increases, reaches a maximum at approximately mid of the contour length and become thinner just before the trailing edge. Near the trailing edge, boundary layer thickness again starts increasing. Typically the boundary layer is laminar up to approximately 28% of contour length on the pressure side. On the suction side boundary layer for smooth surface is laminar up to approximately 82% of the contour length. With roughness of 120 grade and 40 grade emery paper, the momentum thickness increases respectively, by 1.5 and 2 times the thickness with smooth blades, Bammert and Sandstede [1980].

2.12.2 Effect of aspect ratio, pitch chord ratio, Match number and inlet flow angle

Deich, et al. [1965] has presented the performance characteristics of different profiles used in steam turbines. For the same inlet angle, pitch chord ratio and stagger angle, the loss coefficient increases with aspect ratio, also the loss is less for higher Mach number similarly,the loss coefficient decreases with increase in inlet flow angle and for higher aspect ratio the loss for the same Mach number, pitch chord ratio and stagger angle, the loss coefficient also decreases with increase in mach number. The energy loss coefficient for a typical profile is 4.3% at Mach number of 0.6 which decreases to 3.5% when Mach number is increased to 0.9, Keeping other parameters constant. The boundary layer thickness decreases with Mach number (Mee at al.[1992a, b]) in the range of 0.65-0.85. with further increase in the Mach number there is enormous increase in boundary layer thickness due to increase in pressure gradient over the accelerating region near the throat. The wake is asymmetric at the trailing edge, but it becomes near symmetric at a distance away from the trailing edge and centre of the wake curves away from the pressure surface due to static pressure gradient.

Chapter 3

LITERATURE REVIEW (Recent work)

The degradation of turbines with service is a serious problem that must be appropriately addressed for efficient and safe operation. Therefore study of all the parameters affecting the turbine performance become important. The degradation of turbine performance are caused by a wide variety of operational and environmental factors and roughness is one such factor.

Here I am focusing light over the work done on the roughness of turbine blades due to various reasons. The previous work done by various people show the major causes and impact of surface roughness on the turbine blades. Surface roughness is known to have significant effect on the turbine performance by impacting the heat loss and pressure variation. Over the time as turbines are exposed to various loads the external surfaces become rougher, which results into increased heat loads and frictional losses. There have been a number of investigations over the surfaces with uniform or two dimensional roughnesses to understand the pattern of roughness, its causes and realistic effects of this surface roughness on the performance of turbines. The causes and effects of surface roughness on turbine performance are reviewed based on publications in the open literature over the past 60 years. Empirical roughness correlations routinely employed for drag and heat transfer estimates are summarized in various research and paper. No single correlation appears to capture all of the relevant physics for both engineered and service-related (e.g., wear or environmentally induced) roughness. Roughness influences performance by causing earlier boundary layer transition, increased boundary layer momentum loss (i.e., thickness) or flow separation. Roughness effects in the turbine are dependent on Reynolds number, roughness size, and to a lesser extent Mach number.

3.1 Mechanisms of roughness

In turbine roughening of blade surface is caused by erosion, corrosion, and deposition, individually or in tandem due to a variety of physical and chemical phenomena. It result in change in blade profile and roughness over the surface that varies along the blade span as

well as from initial stage to final stage. Brief description on each of these three mechanisms is given below.

3.1.1 Erosion

Erosion is removal of material by cutting and ploughing by particles or local melting of material due to localized high temperature caused by particle impact. In a particular particle target material combination, particle size, impacting velocity, impiningment angle and metal and fluid/gas temperature affect the erosion rate and its location [hammed and fowler 1983]. Tabakoff [1984] observed that erosion increases by 2.5 times when temperature increases from 26°c to 649°c and by 6.5 times when velocity increase from 197m/s to 328m/s. Water drops (50-450µm diameter) present in wet steam impinging on blades and cause erosion mainly at leading edge on either pressure or suction sides, again impact the pressure surface closer to the trailing edge Erosion increases radically to wards the blade tip and increases axially from trailing to leading edge. Metwally et.al [1995] observed that the stator blade suffers maximum erosion at leading edge and trailing edge near the hub where as for the rotor blade maximum erosion occurs mostly at the outermost radial locations. The mechanism of erosion also depends on the growth of the boundary layer over the blade surface and angle of incident.

3.1.2 Deposition

Cotton and Schofield [1971] observed copper salts deposits of 1.0 mm on the nozzles of the first stage and 2.4mm deposits on the 7^{th} stage of a power plant steam turbine. On the rotor blades, deposits varied from 0.3 mm on the1st stage to 0.5 mm on the 4^{th} stage and 0.7 mm on the 7^{th} stage. Water flowing in the steam path through well treated, contains salt that are deposited on various surfaces including turbine blades. These salts deposits (David [1999]) produce roughness's and alter the blade profile causing performance decoration and also affect the natural frequency of balding due to added mass on the blades [stamatis,et al.1999]. the sticking tendency of salts can be controlled by mixing additives in the working fluids which loosen up the deposits.

Figure 3.1 Roughness caused by deposits on turbine blades M/s Encodes

3.1.3 Corrosion

The presence of oxygen, carban dioxide and wetness in steam are responsible for chemical reactions with blade surfaces. This phenomenon produces roughness either due to random thickening of blade profile if the oxidized material adheres to the blade surface or by random thinning if the oxidized material tears off form the blade surface. In the latter scenario, it could also contribute to erosion of downstream stages. Corrosion depends on the electrochemical processes taking place at the boundaries of contact, usually between wet steam and the metal. Povaro of metal consisting of anoding section where metal losses its ion and electrons and cathodic section where electrons are absorbed and hence the rate of corrosion is governed by overall current through the circuit. Magnetite thus formed has matching crystalline lattice parameters and adheres strongly to the blade acting as a protective layer, a process called passivation.

Figure 3.2 Roughness caused by solid particle erosion of turbine diaphragm (NTPC Vindhyachal).

3.2 Roughness Measurement

As previously noted, the surface roughness of real turbine blades can vary significantly. Because of this variation, it is both necessary and helpful to develop an analogous relationship between differing surfaces. In order to do so, several statistical parameters can be applied to characterize each surface. Some of the more common parameters used to describe surface roughness are average centreline roughness, R_a, root-mean-square roughness, R_q, and maximum peak-to-height roughness, R_t. Additional parameters may include surface skewness, Sk, and kurtosis, Ku.

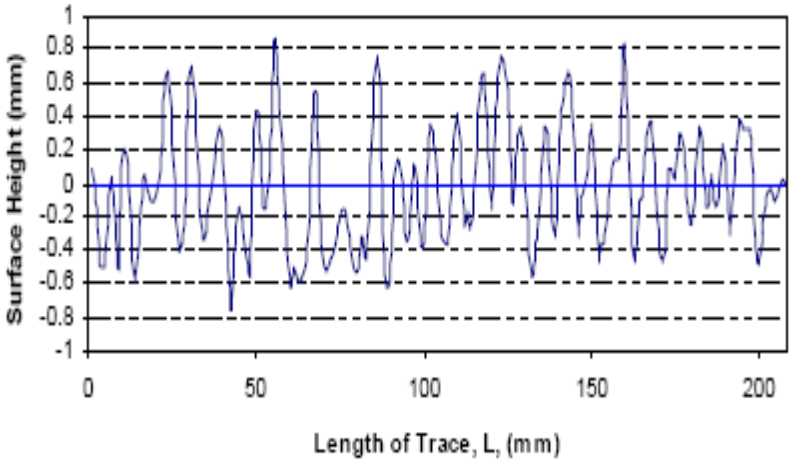

Figure 3.3 Roughness Trace from Erosion Panel Bennett [5]

Average centreline roughness is typically used to describe machined surfaces Bennett [5]. It is measured along a line of length L, and is defined as the mean surface level such that equal areas of surface lie above and below it. The mean surface level can mathematically be written as:

$$\sum_{i=1}^{N} y_i = o \tag{3.1}$$

Where N is the number of elements measured along the trace length L.

Ra is the measure of the variability in a given set of data and provides one with the average of the absolute deviations of the surface heights from their mean. Ra is mathematically given by:

$$R_a = \frac{1}{N}\sum_{i=1}^{N}|y_i| \tag{3.2}$$

The root-mean-square roughness is the most important statistical parameter and is typically used to describe the finish of optical surfaces. It is defined as the square root of the average of the squares of the surface heights from their mean surface level and can be written as:

$$R_q = \sqrt{\frac{1}{N}\sum_{i=1}^{N} y_i^2} \qquad (3.3)$$

Rms roughness, like R_a, is also measured along the trace length L, but is additionally dependent upon the surface area of the measurement and the distance between the elements. Consequently, there is no specific rms value for a given surface.

For surfaces composed of small, consistent roughness elements, R_a and R_q will be very similar. Conversely, if the surface has a significant number of large peaks or valleys, the second order terms in R_q dictate the calculation and R_q becomes larger than R_a

The maximum peak-to-height roughness, R_t, is simply that, a measure of the total size of the elements. It is mathematically written as:

$$R_t = y_{max} - y_{min} \qquad (3.4)$$

where y_{max} is the largest positive deviation from the mean centreline and y_{min} is the largest negative deviation from the mean centreline.

Skewness, S_k, is a characterization of the degree of asymmetry of a surface about its mean centreline and is written as:

$$S_k = \frac{1}{R_q^3}\left[\frac{1}{N}\sum_{i=1}^{N} y_i^3\right] \qquad (3.5)$$

The sign of skewness relates whether the deviations generally lie above or below the mean centreline. Thus, bumps on a surface will result in a positive skewness and pits or holes in the surface will, conversely, result in a negative skewness. It is also noteworthy that skewness, like rms, is greatly governed by its higher order term. As a result, S_k is more sensitive to deviations that lie farther from the mean centreline

Kurtosis is defined as the relative peakedness or flatness of a distribution compared with its normal distribution. A large kurtosis is representative of peaked distributions while a small kurtosis indicates a relatively flat distribution. Kurtosis is defined as:

$$K_u = \frac{1}{R_q^3}\left[\frac{1}{N}\sum_{i=1}^{N} y_i^4\right] \tag{3.6}$$

Yi Liu (2007) has studied the aerodynamics and heat transfer prediction in a highly loaded turbine blade. An efficient numerical method, modified implicit flux vector splitting (MIFVS), has been extended to solve the transonic cascade flow and heat transfer in a highly loaded turbine blade. Key characteristics of the MIFVS solver include the establishment of an implicit formulation, Eigen value analysis of the Jacobi matrices for the NS equations. Since matrix operations are not necessary in the implicit solver, computing efforts in each iteration step can be significantly reduced.

A low Reynolds number k–Ɛ turbulence model, with the compressibility effect considered and the turbulence production term Pk modified near the blunt leading edge, and a transition model have been implemented into the MIFVS solver. Results obtained for the wave profiles, the surface isentropic Mach number distributions, Schlierenimage and heat transfer show good agreements with the experimental data and other published calculation results. The important flow features are well predicted. By simulating this transonic transition flow, the extended MIFVS is demonstrated to be numerically efficient and accurate for the highly loaded turbine blade.[3]

Li Wei and Qiao Weiyang (2008) have studied the tip clearance flows in turbine cascades. In This paper presents detailed measurement and discussion on the tip clearance flow at 40%chord downstream of the cascade exit plane of turbine cascade. It examines the effects of five different tip clearance heights, three different exit Mach numbers and non-uniform tip clearance height upon the tip clearance flow and has drawn the following.

(1) When the tip clearance heights in adjacent blades increase, the tip clearance flow across their tip gap strengthens, so it is with the pressure difference between the

pressure side and suction side in the central passage. Moreover, the loss due to tip clearance flow on central blade increases.

(2) Under the experimental conditions of the study, generally, the total pressure loss proportionally rises with the tip clearance height. The results acquired in the study again evidence the conclusion that in 1.0%*H* case, the total pressure loss Coefficients at different exit Mach numbers are almost equal while in the cases with tip clearance heights of other than 1.0%*H*, the coefficient becomes Higher as the exit Mach number increases.

(3) Comparing with the effect of tip clearance height on tip clearance flow, the effects of exit Mach number and non-uniform tip clearance heights are so tiny that they could be neglected under the conditions of the experiments.[4]

Qiang Xiaoging and Wang sangtao (2008) have studied the aerodynamic design and analysis of a low reaction axial compressor stage. Associated with the boundary layer suction method, a new axial compressor design concept based on highly-loaded, low-reaction and boundary layer suction is proposed in this paper. The limiting factors of this concept are:

(1) The slightly low Mach number after the rotor;
(2) The pre-whirl angle of the rotor;
(3) The separation control method in stator cascade.

The analysis of the low-reaction stage proves the feasibility of the new design concept which is helpful to increase aerodynamic loading. This concept can be used in designing high pressure stages of aero engine, compressor of ground gas turbine exclusive of the transonic stages and high total pressure ratio blower

Sang Woo Lee and Jin Jae Park(2009) have studied the effect of incidence angle on end wall convective transport with in a high turning turbine rotor passage. In this paper investigated. Surface flow visualizations and heat/mass transfer measurements are

carried out at the inlet Reynolds number of2.78 x 10^5 for incidence angles of-10^0, -5^0 0° +5^0, and +10^0. The results are summarized as follows.

(1) The incidence angle has considerable influences on the end wall local convective transport phenomena and on the behaviours of various end wall vortices.
(2) The surface flow visualizations show that in the case of negative incidence, there exists a considerable advancement offend wall separation line with a narrower suction-side corner vortex area, in comparison with the zero incidence case. In the case of positive incidence, there are a slight retreat and minute advancement of the separation line near its ends with a wider suction-side corner vortex area.
(3) The mass transfer data provide that in the case of negative incidence, convective transport is less influenced by the leading edge horseshoe vortex and by the suction-side corner vortex along their loci but is increased along the pressure-side corner vortex. In the case of positive incidence, however, convective transport is augmented remarkably along the leading edge horseshoe vortex, and is much influenced by the suction-side corner vortex. Moreover,
heat/mass transfer is enhanced significantly along the pressure-side leading edge corner vortex.
(4) Local end wall convective transport in the area other than the end wall vortex sites is much influenced by the inlet-to-exit velocity ratio in the cascade passage.
(5) With the increment of the incidence angle from+10^0 to - 10^0,mass transfer Stanton number averaged across the entire end wall region based on the inlet free-stream velocity decreases mildly but that based on the exit mid-span velocity increases more steeply.

Kim Jinwook and Kim Tongbeum (2009) have studied the effect of the leakage flow tangential velocity in shrouded axial compressor cascades. This paper examines the effects of the relative motion between stationary and rotating surfaces (i.e., leakage flow tangential velocity, *vy*/*c*) on the blade passage flows in shrouded axial compressor cascades. The findings of this study are as follows.

(1) A new shrouded compressor cascade facility has-been developed which enables testing of the relative motion effects in a non-rotating environment.

(2) The upstream injection into the mainstream flow of the leakage flow with increasing tangential velocity makes the flow in the passage become more radially uniform and weakens the secondary flow. Thus, the mixing loss between leakage and passage flows is reduced, and the overall loss is reduced.

(3) With increasing leakage tangential velocity, the three-dimensional shape of the loss core, concentrated in the hub suction side corner, becomes more two-dimensional.

Qi Lei and Liu Huoxing (2010) have studied the upstream wake secondary flow interaction in the end wall region of high loaded turbines. The interactions between upstream periodic wakes and secondary flow vortices in the end wall region of a linear turbine cascade and a turbine rotor were investigated by experimental and numerical method. In the cascade case and rotor case.

Cascade case: The flow field at the exit of the cascade showed a decrease in passage vortex strength and loss due to the upstream wake transport. There are two interaction mechanisms that cause the decrease in passage vortex loss. Firstly, the negative jet effect of the wake reduces the momentum difference between the end wall boundary layer and the main flow, which suppresses the development of the pressure side leg of the horseshoe vortex. Secondly, as

the wake passes through the cascade passage, a cross flow toward the blade suction surface arises due to the negative jet effect of the wake, which counteracts the growth of the passage vortex. In addition, the unsteady mixing of the upstream wake in the passage significantly increased the unsteady loss, which has detrimental effect son the performance of the end wall region.

Rotor case: The transport of the upstream stator wakes in the rotor passage significantly changed the secondary vortices structure at the rotor exit. Due to the effect of the wake, the loss core corresponding to the hub passage vortex moves far away from the hub end wall with the maximum loss value decreasing, and the loss core corresponding to the hub wall vortex almost disappears completely. An additional high loss region (Region A) can

be observed due to the effect of the upstream wake, which is the main difference of the effect of upstream wake interaction between in the linear turbine cascade
And in the turbine rotor. The wake transported into the rotor passage can cause a strong disturbance flow with a downward component, and consists of two
Branches with counter rotating vortices. The positive branch continues to reinforce the hub boundary layer and generates high loss region (Region A) finally.

Guo shaung and Chen shaowen (2010) have studied the effect of boundary layer suction an Aerodynamic performance in a high-load compressor cascade. In this paper The loss of a high-load compressor cascade can be reduced by means of boundary layer suction. By increasing the suction flow rate at a proper position, a maximum reduction of 16.5% in the total pressure loss could be achieved in comparison with the cascade without boundary layer suction.
The boundary layer suction at the suction surface brings the wake under effective control and effectuates remarkable loss reduction at the mid span of the flow passage in all the cases under study. The end wall loss reduction is only visually discovered when the suction is applied to where the boundary layer deviates not too far from the blade surface (for instance, Slot 3 and Slot 4).
Low suction flow rates are sufficient for achieving noticeable improvements in performances when the boundary layer is applied at the position near the leading edge. However, in this case, continuing to increase the suction flow rate would result in slim and limited effects. It is evidenced that the proper suction position plays a more active role in reducing the loss of cascade than the suction flow rate. Consequently, it is more important to find out the optimal suction position than to determine the appropriate suction flow rate.

I.A. Hamakhan and T.Korakianitis (2010) have studied the Aerodynamic performance effects of leading edge geometry in gas-turbine blades. this is the first reported attempted to remove the leading edge spikes with a surface-curvature direct blade-design method. It is noted that suction-surface spike and the pressure-surface region of diffusion near the leading edge have been completely removed The results show that the

prescribed surface-curvature distribution blade-design method is a robust tool for blade design, providing a manageable and accurate way to control the blade surface and the aerodynamic properties around the blade.

The prescribed surface curvature blade design technique results in smoother boundary layer flows, affecting aerodynamic as well as heat transfer performance. Sample blades B1, B2 and B3 have been designed to show the capability of the method to eliminate the spike and dips in the surface Mach number distribution at design and off-design conditions in the vicinity of the leading edge circlet both design and off-design conditions. Stagnation pressure losses decrease with smoothing the blending of the circle with the blade surfaces, as predicted by Benner.

We conclude that the prescribed surface curvature blade design technique can be used to provide accurate guidance and control for the design of blade shapes. Furthermore the method can be used to eliminate the flow problems resulting from blending a leading edge circle or other shape with the blade surfaces at design and off-design conditions.

The prescribed-curvature blade design technique has been used to design stacked 3D turbine blades, compressor and fan blades, isolated airfoils, and wind urines. These will be reported in other papers.

Seong Eun Lee and Sang Woo Lee (2011) have studied the tip leakage aerodynamics over stepped squealer in a turbine cascade. In this paper the present investigation the Tip gap flow physics and aerodynamic loss generations for the HPLS and LPHS stepped squealer tips have been investigated for a fixed tip gap height-to-chord ratio of h/c = 2.0% in a turbine cascade.

(1) For the HPLS tip, the incoming leakage flow over the pressure-side rim cannot reach the blade suction side due to the presence of an inlet flow intrusion over the suction-side rim in the upstream region, but it penetrates into the blade flow passage in the downstream region. All over the cavity floor, there exists a strong near-wall flow heading toward the trailing edge.

(2) The LPHS tip has a mid-chord leakage flow penetration into the blade flow passage, and also provides a downstream leakage flow penetration deeper than that for the HPLS

tip. Its cavity floor can be divided into a backward flow region and a wide separation bubble.

(3) The HPLS tip has lower aerodynamic loss than the LPHS tip-in both passage and tip leakage vortex regions. Lower aerodynamic loss in the passage vortex region for the HPLS tip is attributed to the presence of the inlet flow intrusion. Higher aerodynamic loss in the tip leakage vortex region of the LPHS tip results from the further upstream start of the leakage flow discharge and the following deeper downstream leakage flow penetration.

(4) In the reduction of aerodynamic loss mass-averaged all over the measurement plane, the HPLS and cavity squealer tips are better than the LPHS and plane tips, but there is almost no difference in the aerodynamic loss generation not only between the HPLS and cavity squealer tips but also between the plane and LPHS tip.

Dr. Samsher categories the mechanisms of roughness into corrosion, erosion and deposition. They also examined the turbine blades and locate the regions in various stages and over the entire blade length which are prone to corrosion, erosion and deposition. They also explained the reasons of these variations. After characterization of various roughness mechanisms on the blade surface they characterized the roughness patterns at various locations

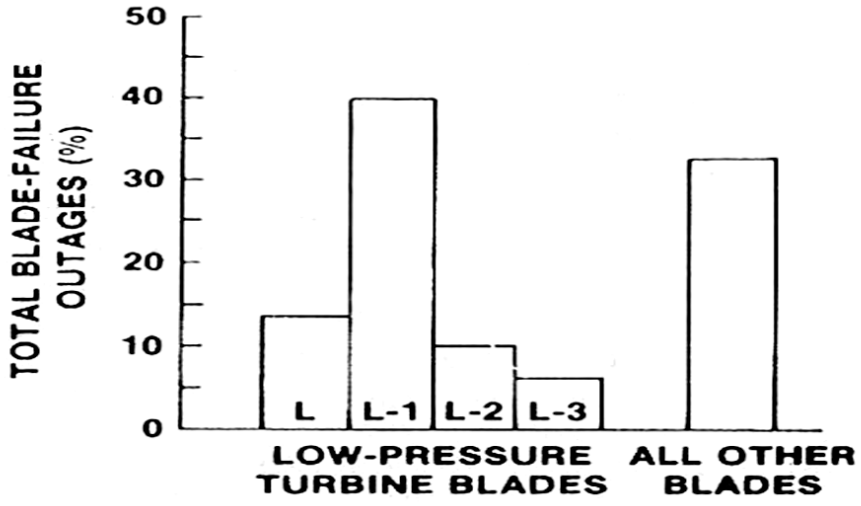

Figure 3.4 the effect of corrosion at various turbine blades

Awatef A. Hamed, Widen Tabakoff, Richard B. Rivir, Kaushik Das and Puneet Arora conducted test in the erosion wind tunnel for coated and uncoated blade materials at various impact conditions. They employed numerical simulations for the three-dimensional flow field and particle trajectories through a low-pressure gas turbine to determine the particle impact conditions with stator vanes and rotor blades using experimentally based particle restitution models. The measurements indicate that both erosion and surface roughness increase with impact angle and particle size. The trajectories indicate that the particles impact the vane pressure surface and the aft part of the suction surface. The impacts reduce the particle momentum through the stator but increase it through the rotor. Vane and blade surface erosion patterns are predicted based on the computed trajectories and the experimentally measured blade coating erosion characteristics.

From the figure 3.4 it is clear that the low pressure blades are susceptible to corrosion.

Experimental results for blade and coating material erosion indicate that both erosion rate and Surface roughness increase with the eroding particle impact velocities and impingement angles and that larger particle produce higher surface roughness. The computational results of particle dynamics simulations indicate that many particles impact the vane pressure surface and that the larger particles cross over and impact the vane suction surface toward the trailing edge. The vane surface impacts reduce the particles' absolute velocity and, consequently, they impact the rotor blade suction surface

In a experimental study, Samsher[1] applied

Three levels of roughness for three different blade profiles. He applied nine different patterns of roughness on the each of the three different blade profiles. He selected the three profiles one nearly, impulse and two of different degree of reaction for testing. Six blades were

The profile loss coefficient increased with increase in roughness; the rate of performance deterioration was high at smaller roughness and it reduced at higher roughness. The entire pressure or suction surfaces with small roughness have comparable detrimental effect; however for higher roughness of 50 grades the detrimental impact was more with the roughness on the suction surface. The shifting of wake towards the

suction surface was maximum when roughness was applied over the entire suction surface and also at mid-chord region of suction surface, whereas shifting of wake towards the pressure surface was less and limited when roughness was applied over the entire pressure surface and localized roughness over the pressure surface.

Figure 3.5 Experimental set up of rectilinear cascade of blade Samsher [1]

The roughness over the entire suction surface was more detrimental than that over the pressure surfaces for all the profiles (impulse as well as reaction). The comparison of loss coefficients with identical roughness over suction surface leading edge, the mid-chord and trailing edge reveals that for higher roughness (50 grade) on impulse and reaction blades (entire blade of a real turbine), mid-chord was most sensitive followed by trailing edge and then leading edge. But for lower roughness values, leading edge region of impulse and high reaction blade was more sensitive than that of trailing edge, whereas for moderate reaction blade, the trailing edge was more sensitive. For similar roughness at identical localized places over the suction surface, the most detrimental location was the root profile followed by mid height section (moderate reaction) and tip. Similarly, for the

pressure surface for higher roughness over the impulse and reaction blade profiles, mid-chord region was least sensitive whereas leading and trailing edge regions were almost equally detrimental. For lower roughness on impulse blades, leading and mid-chord regions were almost equally detrimental and trailing edge region was least sensitive. Similarly, for identical roughness (50 grade) over identical localized places over pressure surface, for root section was most sensitive followed by higher reaction and then moderate reaction.

The non uniformity of flow in pitch wise direction at the exit of a row of blades has undergone a considerable increase with increase in level of roughness over the blades for each profile compared to the corresponding smooth blades. This was the result of the combined effect of increased roughness and thicker trailing edges.

As the discharge pressure was low, the experiment could not be carried out at higher Reynolds numbers and higher Mach numbers. Also data on skin friction, turbulence kinetic energy, turbulence intensity, Mach number at all locations is not available.

Hamed has been investigated the turbine vane and blade material surface deterioration caused by solid particle impacts. The tests were conducted in wind tunnel for coated and uncoated blade materials at various impacts conditions. Surface roughness measurements obtained prior and subsequent to the erosion tests were used to characterize the change in roughness caused by erosion. With the help of experiment based particle restitution models, numerical simulations for the three dimensional flow field and particle trajectories through a low pressure gas turbine were employed to determine the particle impact conditions with stator vanes and rotor blades.

The measurements indicated that both erosion and surface roughness increase with impact angle and particle size. Turbine vane and blade surface deterioration was strongly dependent on the turbine geometry, blade surface material, and particle characteristics. Experimental results indicated that erosion rate and surface roughness increase with the eroding particle impact velocities and impingement angles and that large particle produce higher surface roughness. Prediction based on the computed particle trajectories and the experimental characterization of coated vane material indicated a narrow band of high

erosion at the vane leading edge and pressure surface erosion increasing towards the trailing edge.

Hummel *et al.* [7] evaluated the aerodynamic performance of a turbine blade via total pressure loss measurements on a linear cascade. The Reynolds number was varied from 600,000 to 1,200,000 to capture the operating regime for heavy-duty gas turbines. Four different types of surface roughness's on the same profile were tested in the High Speed Cascade Wind Tunnel of the University of the German Armed Forces Munich and evaluated against a hydraulically smooth reference blade. The ratios of surface roughness to chord length for the test blade surfaces were in the range of $7.6x10^{-06}$ to $7.9x10^{-05}$. The total pressure losses were evaluated from wake traverse measurements. The Reynolds number dependency was measured.

It was found that maximum loss increases due to surface roughness that occurred at the highest Reynolds number tested. Maximum loss increases due to the highest surface roughness analyzed was 40% at nominal flow conditions compared to a hydraulically smooth reference blade. In addition to the tests a comparison to a loss model according to literature showed good agreement to both the results from this test series and further data from literature.

Zhang has been investigated the effects of surface roughness on the aerodynamic performance of a turbine vane for three Mach number distributions (where M = 0.35 to 0.71), one of which resulted in transonic flow and matched an arrangement employed in an industrial application. Four turbine vanes, each with the same shape and exterior dimensions, were employed with different rough surfaces. The non-uniform, irregular, three-dimensional roughness on the tested vanes was employed to match the roughness which existed on operating turbine vanes subjected to extended operating times with significant particulate deposition on the surfaces. Wake profiles were measured for two different positions downstream the vane trailing edge.

The wakes become broader with increased roughness size or with increased exit Mach number M_{ex} due to higher advection velocities, augmentations of mixing and turbulent transport, thicker boundary layers, earlier laminar-turbulent transition and increased

turbulent diffusion. Peak values of total pressure loss coefficients also increased dramatically as M_{ex} increases. In general, these profiles were asymmetric because the effects of surface roughness were much less apparent for positive y/c_x values, downstream of the pressure sides of the vanes. This was due to different loading, different boundary layer growth, and different susceptibility to flow separation on the different vane surfaces, which also caused the suction side wakes (at negative y/c_x) to be thicker than the pressure side wakes (at positive y/c_x). Overall, the wakes were pushed toward smaller y/c_x values as they were advected downstream (i.e. towards the vane suction side), regardless of the level, uniformity, or variability of the roughness along the

surfaces of the vanes. Aside from this, the data from a vane with variable surface roughness showed different quantitative and qualitative trends compared to profiles measured downstream of vanes with roughness spread uniformly over the surfaces. This was partially due to different rates of boundary layer development as different levels of roughness were encountered along the vane pressure surface.

Magnitudes of area-averaged loss coefficients Y_A generally increased as either exit Mach number or equivalent sand grain roughness size increased. The increases in Y_A magnitudes were especially substantial as the exit Mach number increases from 0.5 to 0.7 for the smooth vane and the uniformly-roughened vane with k_s/c_x = 0.0108. Mass-averaged loss coefficients Y_p showed similar trends, since they also increased as normalized mean roughness height became larger for a particular value of vane exit Mach number.

Zhang has been determined the skin friction coefficients from wake profile measurements. The method was applied to symmetric turbine airfoils with rough surfaces, which operate in a compressible, high-speed flow environment with Mach numbers in the free-stream flow just adjacent to the airfoil ranging from 0.35 to 0.70. The roughness employed simulates that which develops on operating turbine airfoils, over long operating times, due to particulate deposition and due to spallation of thermal barrier coatings. Surface roughness was characterized using equivalent sand grain roughness size. Magnitudes of normalized equivalent sand grain roughness for the smooth airfoil and two rough airfoils were 0, 0.00069, and 0.00164.

For the present airfoil, it was found that because of larger surface roughness elements give thicker boundary layers at the airfoil trailing edge as a result of higher turbulence transport levels and higher rates of free-stream fluid entrainment. According to FLUENT 6.0 simulations, the differences in flow separation extent and initiation near the airfoil trailing edge due to changing surface roughness were very small for the present symmetric airfoil. Numerical predictions also indicated that the flow around each of the airfoils

tested was fully turbulent or nearly fully turbulent along the length of each airfoil.

With the same inlet experimental condition for each case, skin friction coefficients for the rough airfoils, determined from the wake profiles of stream-wise momentum, increased considerably as the magnitude of normalized equivalent sand grain roughness size increased. For an inlet turbulence intensity level of 0.9%, the skin friction coefficients for the smooth and two roughened airfoils were 0.00192, 0.00637, and 0.00986, respectively. The numerical prediction of the overall skin friction coefficient for smooth airfoil was determined by using FLUENT 6.0 software.

The present skin friction determination technique was useful for any sort of body in which different levels of surface roughness were considered. Here, the values obtained were mostly due to surface shear stress forces along the airfoils, however, the technique can be extended to also include the influences of flow separation and form drag.

C.R.F. Azevedo, A. Sinátora investigated the hydroelectric steam turbine rotor using visual inspection, non-destructive testing, macro and microfractography, microstructural characterization, EDS microanalysis, chemical analysis, micro hardness and tensile testing. The blades belonged to the last stage turbine generator indicated that foreign-particle erosion, which attacked at the low-pressure side of the lower trailing edge of the blades.

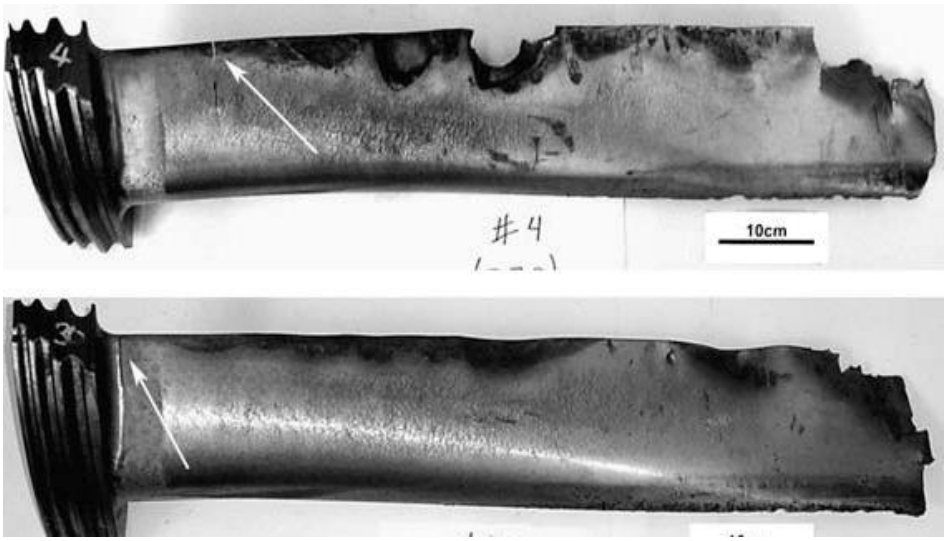

Figure 3.6 material removal due to erosion at the trailing edge of the blade

B.S. Mann studied the erosion in the steam turbine. The erosion is due to the formation of magnetite on the inside of boiler tubes. This builds up, spalls and travels along with the steam causing erosion in areas where steam velocities are the highest. The steam velocities are the highest in the high pressure sections of steam turbines. He concluded that erosion rate depends upon the flow rate and base metal. He predicted the erosion-prone areas of steam turbine blading can be predicted using a simple rotating disc apparatus. From the experimental study, he observed that the erosion-prone areas of steam turbine blades are on the suction side towards the leading edge and on the pressure side; these are towards the trailing edge.

J.W Harpster, recognized that corrosion of copper bearing tubes on the shell side of condensers which act as a contributor to copper deposition on turbine blades. The resulting copper deposits cause loss of load due to a lowering of turbine energy conversion efficiency. Both rotating and stationary blades are affected and the copper thickness can be up to1/16". Load loss or excess fuel usage to maintain load can exceed 4%.

Kang *et al.* [16] numerically investigated the blade roughness effects on performances and flows of axial compressor and axial turbine stages. A wall function option for roughened wall boundary condition was available in TascFlow code. Flow calculations on the flat plate with various roughness showed that normalized wall velocity drop due to roughness was coincidence with that of Prandtl-Schlichting's empirical relation.

One-dimensional analyses were carried out to inspect the contributions of absolute flow angles and loss coefficient. The boundary layer thickness becomes thick with the roughness so that the boundary layer constricted flow passage to change flow angles at the inlet and outlet and resulted in extra pressure loss. They observed that even a small amount of roughness in compressor critically affect the performance. Rather when roughness height was sufficiently high enough to be in the fully rough regime, the performance values became less sensitive to roughness. There were also similar reports of sensitivity of the performance to small roughness height. For the turbine, efficiencies decreased as the roughness height was increased, while work coefficients show opposite trend. Efficiency drop due to roughness was also completely affected by the loss generation.

Behera [2] performed a computational study of rectilinear blade cascade using the same reaction blade profile used by Samsher in his experimental setup with the help of commercially available software code Fluent. He had applied a Reynolds number of 4.5 x 10^5 at the exit. Mass average loss coefficient, static pressure coefficient over blade surface for different level of roughness (applied over the entire blade surface) was computed and results were compared with the Samsher's experimental results and were found to have a very good agreement. From

Experiment one cannot find skin friction, turbulence kinetic energy, turbulence intensity, Mach number at all location for analysis but with the help of computation methods these all can be studied.

For smooth blades the total pressure obtained from the computational method in the wake zone was lower than experimental values by 6.5 %. The width of wake obtained by simulation was more than the experimental results. The exit angle was comparable at

core flow region but slightly deviate at the wake zone. The average exit angle at measurement plane obtained from experiment was 63° as against 59° from computation.

For rough blades with 100 µm roughness over the entire surface predicted static pressure exhibited a good match with experimental results, barring a few points in the semivaneless region. For the total pressure it was observed that the wake from computation was different from that obtained from the experiment. The experimental wake width was wider than the computational wake and core flow region was more affected in the experiment than the computation. For the profile loss peak values from the computation were higher than experiment in the wake region.

The skin friction coefficient increased with increase in the level of roughness. Width of the maximum skin friction coefficient also increased towards the leading edge, with increase in level of roughness. This was due to the boundary layer that got thickened from the leading edge for higher level of roughness. So the thickening of boundary layer over the blade surface contributed a major loss component in the profile loss of the blade channel. The effect of roughness on skin friction coefficient was more prominent in suction surface than the pressure surface of the blade. The influence of roughness on skin friction coefficient at leading edge was prominent, because of growth of boundary layer due to adverse pressure gradient experienced at leading edge. In major portion of the pressure surface fluid flowed smoothly with favourable pressure gradient, so skin friction coefficient was small. At the trailing edge of pressure surface, the skin friction coefficient increased again due to thickening of boundary layer. With the increase in roughness, the inlet total pressure increased, where as the down stream total pressure decreased

It was observed that the upstream pressure increased with increase in roughness, the variation of total pressure increase with increase in distance was not much. At the stagnation point the total pressure also increased with increase in level of roughness. It was observed that the total pressure at wake zone reduced with increase in level of roughness. For a smooth blade the total pressure at minimum energy point was 96,000 Pa, it reduced to 90,000 Pa for 100 µm blade roughness and it further reduced to around 87,000 Pa at 200 µm blade roughness. Also the low pressure area increased with increase in the level of roughness.

The computation was not carried out for higher level of roughness as it was limited only up to 178 μm. Also the modelling was not done for higher Reynolds numbers and Mach numbers under which are realistic for operating turbines.

Funazaki et al. (1996) investigated the effect of wake passing on the time and span averaged film effectiveness on a _lm cooled blunt body model in a low speed wind tunnel. The wakes were again generated by a rotating bar mechanism. The effect of wake passing on the time and span averaged film effectiveness was miniscule except for the lowest blowing rate condition, where he presence of wakes decreased the film effectiveness on the downstream part of the suction side by about eight percent. It is unclear what the motivation behind the research could have been since actually it is a further implication compared to the experiments done at Texas A & M three years earlier. The use of liquid crystals for the determination of film effectiveness may have been an incentive. Texas A & M used this technique one year later on their setup.

Headman et al. (1997) presented experimental work on a somewhat more realistic model. An annular stationary cascade with an inlet Mach number of 0.27was used to investigate the effect of wake passing on a _lm cooled turbine blade. The wakes were generated using a rotating bar mechanism rotating upstream of the cascade annulus. Showerhead _lm cooling was applied through two rows of holes on both the pressure and suction side and one row in the stagnation line. There was no transition on the suction side with or without wake passing. The effects produced by the wake generator were twofold. On the one hand, the presence of the wakes
generally increased mixing and therefore decreased the film cooling effectiveness all along the blade. On the other hand, the wake generator also generated flow swirl. This flow swirl caused the stagnation line on the rotor blades to move toward the suction side, thereby causing the amount of coolant flow to decrease on the suction side and to increase on the pressure side. This effect attenuated the effect of increased mixing on the pressure side. The decrease of film effectiveness was therefore smaller on the pressure side. On the suction side the decrease was more pronounced due to this shift of coolant flow. Neglecting the effect of the swirl introduced by the wake generator, the decrease of _lm effectiveness was not very significant. The effects of

the wake passing on the time averaged heat transfer were not reported. It can be expected, though, that the effect will be minor since the wakes do not a effect transition on the suction side.

It can be concluded for literature review that experiment investigated of roughness effect has been discussed quite good but computation study of effect of roughness is net sufficiently done. Their in the present work the reports have been made to cover this concept.

Chapter 4

MODELING OF CASCADE

4.1 Description of computational domain

The present work is to determine the profile losses on a rectilinear cascade with various levels of roughness over blade surface computationally using commercially available software FLUENT® code. The FLUENT® code is based on finite volume technique and collocated grid method is used to compute the flow domain. The wind tunnel consists of five flow channels using six test blades placed in rectilinear cascade test section with appropriate stagger angle, chord, pitch, and inlet fluid flow angle and inlet/outlet section for fluid (air) to flow as shown in Figure 4.1, 4.2 and 4.3. The coordinates of all the three profiles are given in Appendix 1.

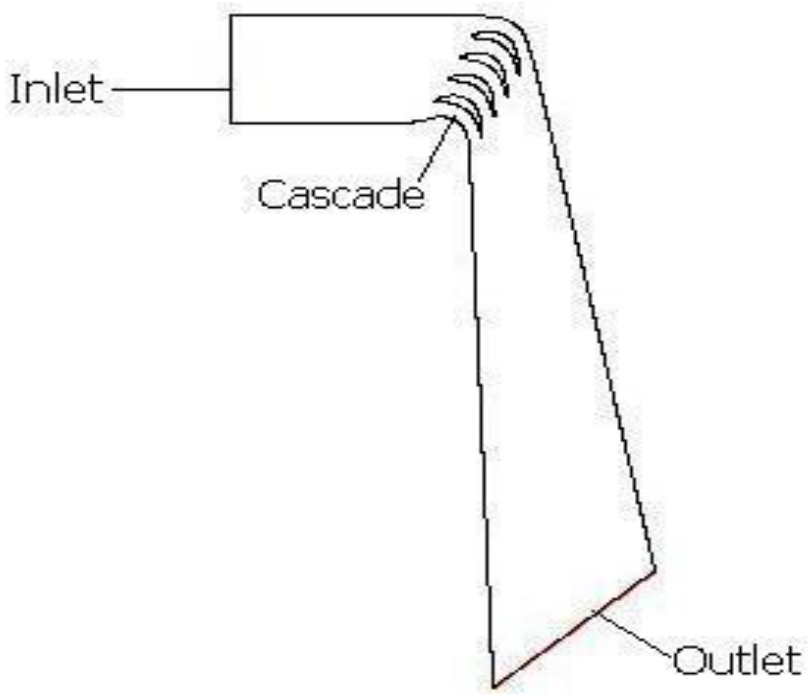

Figure 4.1 Shape of turbine blade 6030 cascade model Samsher [1].

Profile 6030 and Profile 5530 are from last stage of LP turbine and are reaction type, Profile 6030 is from the root of the blade and Profile 5530 is at distance of 30% of

blade height from the root. Profile 3525 is from the first stage of HP turbine and is of reaction type. A 2 dimensional model of all the three profiles was created, with the help of Gambit® and the dimensions of the model were kept same as the experiment performed by Samsher [1] from inlet measurement plane to exit of the tunnel.

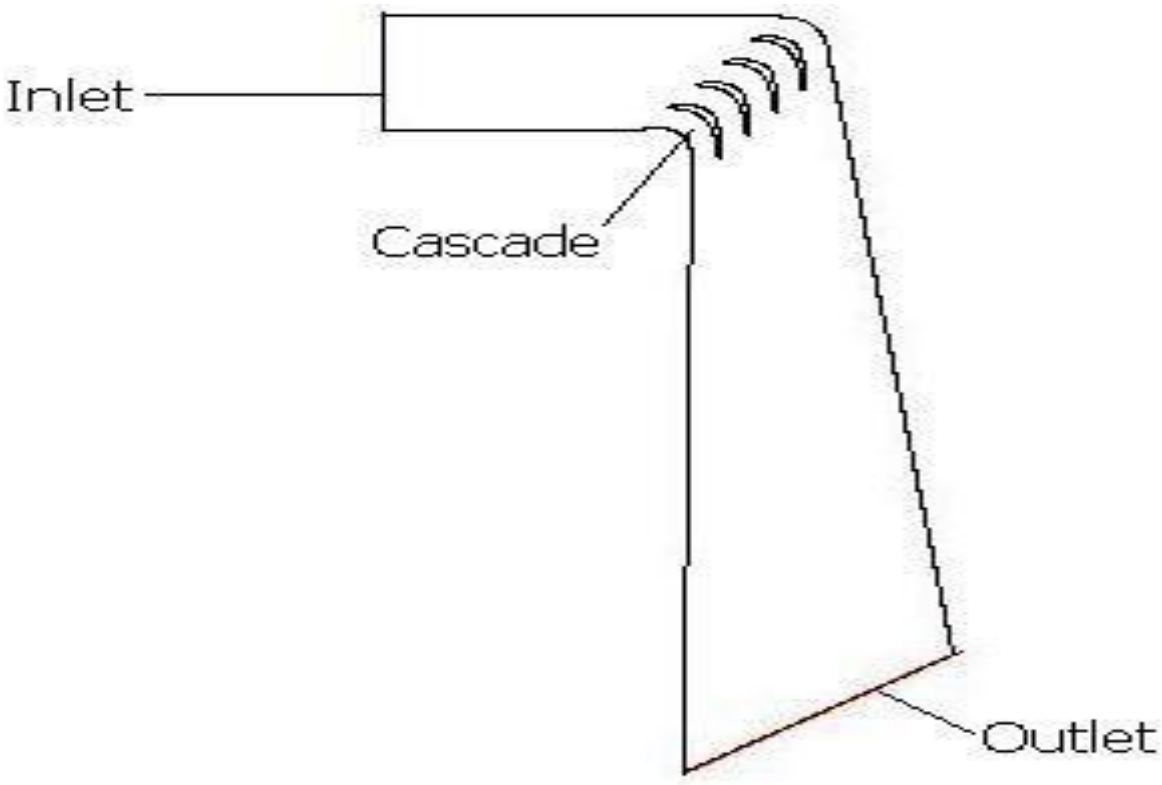

Figure 4.2 Shape of turbine blade 5530 cascade model Samsher [1].

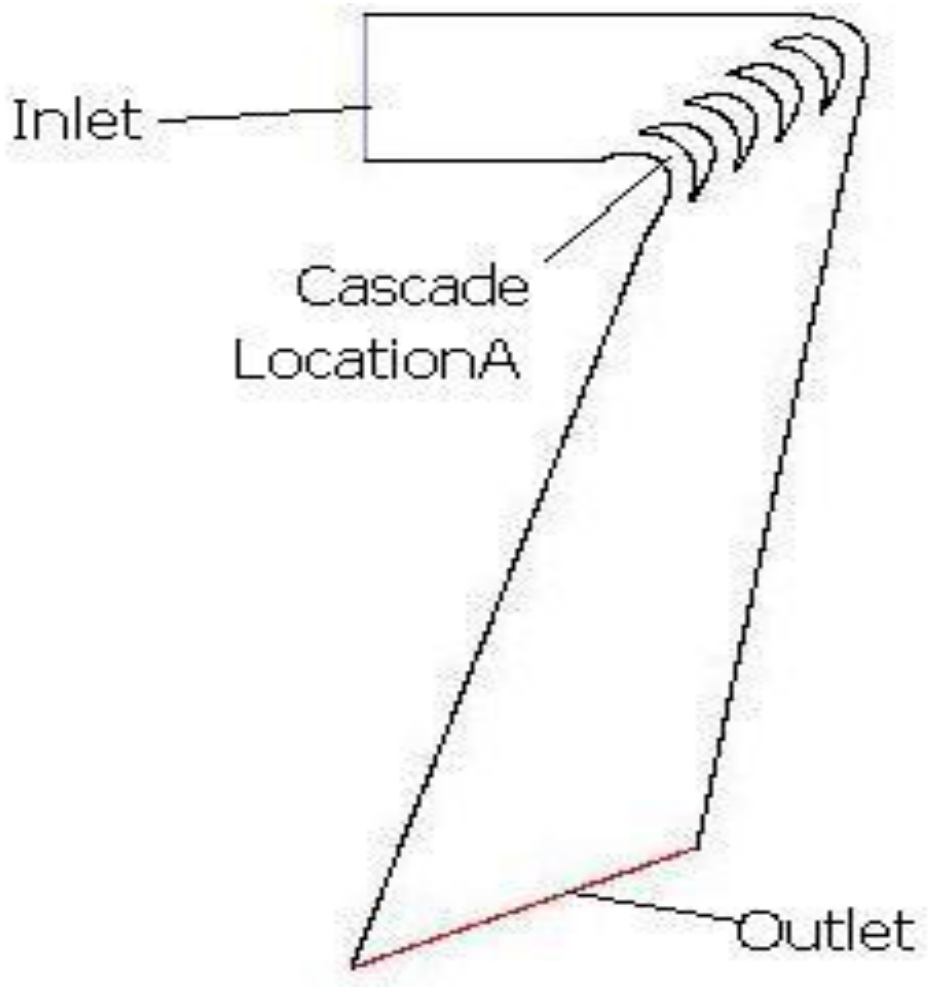

Figure 4.3 Shape of turbine blade 3525 cascade model Samsher [1].

The model was divided into five parts and then each part was again divided in to three parts. Then fine meshing (Quad-Map) was done on the model keeping aspect ratio and equi-skewness angle under control. The meshing of the curved portion of the cascade of the profile 3525 is shown in figure 4.3 after the completion of model, the quality of mesh was checked in the Fluent®. Then simulation was carried out by two dimensions double precision method. The details of the options used on model in Fluent® are described in Appendix 3. The input data used in computation is given in Appendix 4. Mass average loss coefficient, total and static pressure coefficient over blade surface for different level of constant roughness were calculated with the help of commercially available software fluent. With appropriate boundary condition, the flow field was solved for different levels of roughness and results were compared with corresponding experimental Samsher [1] data.

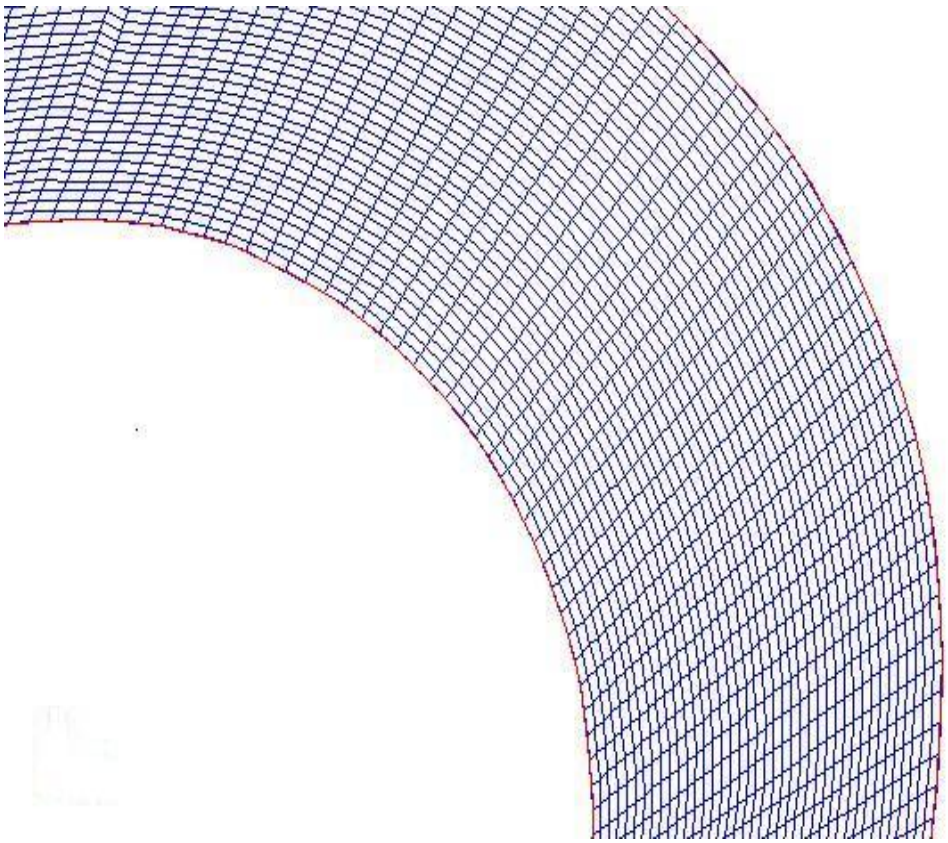

Figure 4.4 Meshing of the curved surface of Profile 3525 at location A.

Table 4.1 Cascade dimensions and flow parameter.

Parameters	**Cascade of blade profile**		
	Profile 6030	Profile 5530	Profile 3525
Cascade type	Rectilinear	Rectilinear	Rectilinear
Inlet cross section	95 x 99.7 mm^2	95 x 94.6 mm^2	95 x 93.2 mm^2
Type of test blade	Reaction type	Reaction type	Impulse type
Chord (mm), c	50	50	50
Pitch (mm), S	22	24	29
Height (mm), l	95	95	95
Blade stagger angle	70°	72	80

Inlet flow angle	65°	52°	40°
Number of blades	6	6	6
Number of channels	5	5	5
Working fluid	Air	Air	Air
Inlet air temperature	30°C	30°C	30°C
Reynolds number at ex (R_{e2})	4.7×10^5	5.0×10^5	3.6×10^5
Roughness level	0 to 500 µm	0 to 500 µm	0 to 500 µm

4.2 Modelling with extra layer of thickness

In the experiment the roughness on the model was provided by the pasting emery papers of different grades on the smooth blade surface. The thickness of emery papers of Grade 220, 100 and 50 was 0.35 mm, 0.44 mm and 0.76 mm respectively. The nine different patterns of roughness were modeled These were complete blade surface, complete suction and pressure surface and one third each of pressure and suction surface at leading edge, mid chord and the trailing edge. Separate model was developed for each pattern of roughness. This thickness was added to the different positions in order to simulate same model for the computational work. The original profile and the extra layer of thickness are shown in figure 4.5.

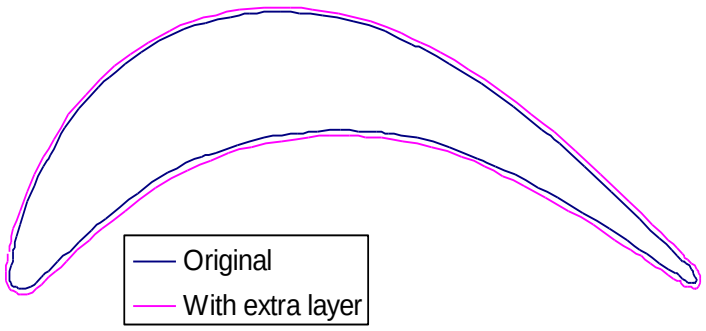

Figure 4.5 Profile 6030 original and with 0.35 mm of extra layer on surface

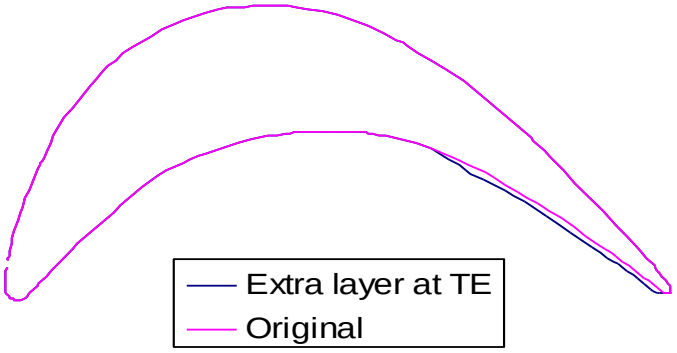

Figure 4.6 Profile 6030 original and with 0.35 mm of extra layer on 1/3rd at trailing edge of the pressure surface.

4.3 The Governing equations

The fundamental governing equations solved for the fluid are as follows:-

1. The continuity equation.
2. The momentum equation.
3. The energy equation.

4.3.1 Continuity equation

The general continuity equation in tensor notation is expressed as:-

$$\frac{\partial \rho}{\partial t} + \frac{\partial}{\partial x_i}(\rho u_i) = S_m \tag{4.1}$$

The equation 3.1 is valid for both incompressible as well as compressible flow. If the flow in which the density of the fluid remains constant, then the continuity equation reduces to

$$\frac{\partial}{\partial x_i}(\rho u_i) = S_m \tag{4.2}$$

Where, ρ is the density of the fluid, $\frac{\partial}{\partial xi}$ is the divergent operator, u_i is the velocity vector of the fluid and S_m is the source term.

4.3.2 Momentum equation

The conservation of momentum in an inertial reference frame in Cartesian coordinate system is expressed as:-

$$\frac{\partial}{\partial t}(\rho u_i) + \frac{\partial}{\partial x_j}(\rho u_i u_j) = -\frac{\partial p}{\partial x_j} + \frac{\partial \tau_{ij}}{\partial x_j} + \rho g_i + F_i \qquad (4.3)$$

Where p is the static pressure, ρg_i is the gravitational body force, F_i is the external body force and τ_{ij} is the stress tensor (which is expressed as below).

$$\tau_{ij} = \left[\mu \left(\frac{\partial u_i}{\partial x_j} + \frac{\partial u_j}{\partial x_i} \right) \right] - \frac{2}{3} \mu \frac{\partial u_i}{\partial x_j} \delta_{ij} \qquad (4.4)$$

Where μ is the molecular viscosity and the second term on the right hand side is the effect of volume dilation and δ_{ij} is the Kronecker's delta.

The value of δ_{ij} = 0 if, $i \neq j$ = 1 if, i=j.

4.3.3 Energy equation

The conservation of energy equation is expressed as:-

$$\frac{\partial}{\partial t}(\rho E) + \frac{\partial}{\partial x_i}(u_i(\rho E + p)) = \frac{\partial}{\partial x_i}\left(k_{eff} \frac{\partial T}{\partial x_i} - \sum_{j'} h_{j'} j_{j'} + u_j (\tau_{ij})_{eff} \right) + S_h \qquad (4.5)$$

Where k_{eff} is the effective conductivity ($k+k_t$, where k_t is the turbulent thermal conductivity) and $j_{j'}$ is the diffusion flux of species j'. The first three terms on the right hand side of energy equation represent energy transfer due to conduction, species diffusion and viscous dissipation respectively. S_h source term if any includes heat of chemical reaction.

The energy term 'E' is further expanded as

$$E = h - \frac{p}{\rho} + \frac{u_i^2}{2} \tag{4.6}$$

Where sensible enthalpy 'h' is defined as

For ideal g

$$h = \sum_{j'} m_{j'} h_{j'} \tag{4.7}$$

And for incompressible flows

$$h = \sum_{j'} m_{j'} h_{j'} + \frac{p}{\rho} \tag{4.8}$$

$m_{j'}$ is the mass fraction of species j' and enthalpy $h_{j'}$ is expressed as

$$h_{j'} = \int_{T_{ref}}^{T} c_{p,j'} dT \tag{4.9}$$

In addition to the above three basic equations of flow, some other equations are also solved depending on the nature of flow phenomenon involved in the problem. For example, if swirling flow takes place in the flow domain, then axial and radial momentum conservation equations are to be solved, where the swirl velocity is included in the equation. Similarly, viscous heating (dissipation) is important for compressible flows, PDF model in energy equation for combustion process, energy source term for chemical reactions, Boussinesq model for natural convection etc. The numerical solution of the

three basic equations of fluid flow gives a close approximation to the flow problem for a steady and laminar flow. Most of the flow occurring in nature and engineering applications is turbulent. So treatment for turbulence is required to have better solution to the problem.

4.4 Turbulence models

Turbulent flows are highly irregular, unsteady, and chaotic and always occur at high Reynolds number. Turbulence is rotational and three dimensional and it is characterized by high level of fluctuating vorticity. Turbulent flows are characterized by fluctuating velocity fields. These fluctuations mix transported quantities such as momentum, energy and species concentration and cause the transported quantities to fluctuate. The instabilities are related to the interaction of viscous terms and non linear inertia terms in the equations of motion. This interaction is very complex: the mathematics of non linear partial differential equation has not been developed to a point where general solutions can be given. The fluctuation of the transported quantities are of small scale and high frequency, they are too computationally expensive to simulate directly in practical engineering calculations. So the instantaneous governing equations are time averaged, ensemble-averaged, or otherwise manipulated to remove the small scales, which give a modified set of equations which are less expensive to solve numerically. But the modified equations contain additional unknown variables for which turbulence models are required to determine these unknown quantities in terms of known quantities.

The most common used approach to address the turbulence effect on flow is the Reynolds Averaged Navier-Stokes equation. The Reynolds Averaged Navier-Stokes (RANS) equation represents transport equations for the mean flow quantities only, with all the scales of the turbulence being modelled. The approach of permitting a solution for the mean flow variable greatly reduces the computational effort. A computational advantage is seen even in transient situations, since the time step will be determined by the global unsteadiness in the mean flow rather than by the turbulence. This approach is generally

adopted for engineering calculations. The most commonly used model κ-ε and its variants, κ-ω and its variants, Spallart-Allmaras and the Reynolds stress model (RSM) adopted the RANS approach for solving turbulent flow field.

In RANS approach, the solution variables in the instantaneous Navier-Stokes equations are decomposed into the mean (ensemble-averaged or time averaged) and fluctuating components. The velocity component in tensor notation (3d) is expressed as

$$u_i = \overline{u_i} + u_i' \tag{4.10}$$

Where $\overline{u_i}$ and u'_i are the mean and instantaneous velocity components

Similarly for scalar quantities:

$$\phi = \bar{\phi} + \phi' \tag{4.11}$$

Where ϕ denotes a scalar quantity such as pressure, energy, species concentration.

Putting the values of flow variable into the instantaneous continuity and momentum equation, the simplified equations are expressed as:

$$\frac{\partial \rho}{\partial t} + \frac{\partial}{\partial x_i}(\rho u_i) = 0 \tag{4.12}$$

$$\rho \frac{Du_i}{Dt} = -\frac{\partial p}{\partial x_i} + \frac{\partial}{\partial x_j}\left[\mu\left(\frac{\partial u_i}{\partial x_j} + \frac{\partial u_j}{\partial x_i} - \frac{2}{3}\delta_{ij}\frac{\partial u_l}{\partial x_l}\right)\right] + \frac{\partial}{\partial x_j}\left(-\rho\overline{u_i' u_j'}\right) \tag{4.13}$$

The above continuity and momentum equations have the same general form as the instantaneous Navier-Stokes equations. Additional terms now appear that represent the effects of turbulence, is called Reynolds stresses, $\rho\,\overline{u'_i\,u'_j}$ and must be modelled in order to close the modified momentum equation.

4.4.1 The realizable k-ε model

The Realizable κ-ε turbulence model has been selected for the solution of present problem (simulation of wind tunnel). The realizable κ-ε model is a relatively recent development. This model is different from standard κ-ε model in two aspects, this model contains a new formulation for the turbulent viscosity and a new transport equation for the dissipation rate, ε , has been derived from an exact equation for the transport of the mean square vorticity fluctuation. From the name of the model it indicates that the model satisfies certain mathematical constraints on the Reynolds stresses, consistent with the physics of turbulent flow. Other two κ-ε models are not realizable. The benefits of realizable κ-ε model is that it predicts more accurately the spreading rate of both planar and round jets. This model provides superior performance for flows involving rotation, boundary layers under strong pressure gradient, separation and recirculation (as in case of flow past aerofoil). Initial studies have shown that the realizable model provides the best performance of all the κ-ε model versions for several validation of separated flows and flows with complex secondary flow features.

The modeled transport equations for κ and ε in the realizable κ-ε model are:

$$\frac{\partial(\rho k)}{\partial t}+\frac{\partial}{\partial x_j}(\rho k u_j) = \frac{\partial}{\partial x_j}\left[\left(\mu+\frac{\mu_t}{\sigma_k}\right)\frac{\partial k}{\partial x_j}\right] + G_k + G_b - \rho\varepsilon - Y_M + S_k \qquad (4.14)$$

and

$$\frac{\partial(\rho\varepsilon)}{\partial t}+\frac{\partial(\rho\varepsilon u_j)}{\partial x_j} = \frac{\partial}{\partial x_j}\left[\left(\mu+\frac{\mu_t}{\sigma_k}\right)\frac{\partial \varepsilon}{\partial x_j}\right] + \rho C_1 S\varepsilon - \rho C_2 \frac{\varepsilon^2}{\kappa+\sqrt{\nu\varepsilon}} + C_{1\varepsilon}\frac{\varepsilon}{\kappa}C_{3\varepsilon}G_b + S_\varepsilon$$

here $C_1 = \left[0.43, \frac{\eta}{\eta+5}\right]$, $S = \sqrt{2S_{ij}S_{ij}}$ and $\eta = S\kappa/\varepsilon$ (4.16)

In the above equations G_k is the turbulent kinetic energy due to mean velocity gradients, G_b is the generation of turbulent kinetic energy due to buoyancy, Y_M is the contribution of fluctuating dilatation in compressible turbulence to the overall dissipation rate, C_2 and $C_{1\varepsilon}$ are constants, σ_κ and σ_ε are the turbulent Prandtl number for κ and ε respectively. These values are computed as follows

$$G_k = -\rho\overline{u'_i u'_j}\frac{\partial u_j}{\partial x_i} \quad (4.17)$$

$$G_b = \beta g_i \frac{\mu_t}{\mathrm{Pr}_t}\frac{\partial T}{\partial x_i} \quad (4.18)$$

and β is computed as $\beta = -\frac{1}{\rho}\left(\frac{\partial \rho}{\partial T}\right)_p$ (4.19)

For ideal gases the term is expressed as

$$G_b = g_i \frac{\mu_t}{\rho \mathrm{Pr}_t}\frac{\partial \rho}{\partial x_i} \quad (4.20)$$

$$Y_M = \rho\varepsilon 2M_t^{\,2} \quad (4.21)$$

$\mu_t = \sqrt{\frac{\kappa}{a^2}}$ where is a is speed of sound (a = $\sqrt{\gamma RT}$)

4.5 Modelling of roughness

When the roughness height is less than viscous sub-layer then the surface is called hydro dynamically smooth surface. Modelling of wall roughness was done using the law of the wall. Wall roughness has little influence upon laminar flow. In turbulent flow, however, even a small roughness will break up the thin viscous sub-layer and greatly increase the wall friction. Experiments in roughened pipes and channels indicate that the mean velocity distribution near rough walls, when plotted in semi logarithmic scale, has the same slope (1/k) but a different intercept. Thus, the law of the wall for mean velocity modified for roughness may be written as

$$\frac{u_p u^*}{\tau_w/\rho} = \frac{1}{k}\ln\left(E\frac{\rho u^* y_p}{\mu}\right) - \Delta B \quad (4.22)$$

Where $u^* = C_\mu^{\frac{1}{4}} \kappa^{\frac{1}{2}}$ and ΔB is a roughness function that quantifies the shift of intercept due to roughness effect. ΔB depends, in general, on the type and size of roughness. For a sand grain roughness ΔB can be well correlated with the non-dimensional roughness height

$$k^+_s = \rho K_s u^* / \mu \tag{4.23}$$

Where K_s is the physical roughness height and

$$u^* = C_\mu^{\frac{1}{4}} \kappa^{\frac{1}{2}} \tag{4.24}$$

The whole roughness regime is sub divided into three regimes viz. hydro dynamically smooth, transitional and fully rough regime. And the value of ΔB is calculated by following formulae

For the hydro dynamically smooth regime (k_s^+ < 3~5)

ΔB = 0

Transitional regime (2.25 < k_s^+ < 90)

$$\Delta B = \frac{1}{k} \ln\left[\frac{K_s^+ - 2.25}{87.75} + C_{K_s} K_s^+\right] \times Sin\{0.4258(\ln K_s^+ - 0.811)\} \tag{4.25}$$

And for the full rough regime (k_s^+ > 90)

$$\Delta B = \frac{1}{k} \ln(1 + C_{K_s} K_s^+) \tag{4.26}$$

The modified law of the wall is then used to evaluate the shear stress at the wall and other wall functions for the mean temperature and turbulent quantities. For assigning the value of roughness constant K_s in FLUENT®, unfortunately a clear guide line is not available. But there is some experimental evidence for non uniform sand grain, ribs and wire mesh roughness, the value of the roughness constant K_s of 0.5 to 1 is more appropriate. When modelling of roughness is to be included, the mesh size has to be

taken care of. For best result, the mesh height near to wall should be more than the roughness height K_s.

4.6 Boundary and operating conditions

4.6.1 Boundary conditions

Boundary conditions specify the flow and thermal variable on the boundaries of the physical model. Therefore, boundary conditions are critical components of the simulation and are important that the boundary conditions be specified appropriately. The simulation shows that the Mach number through the channel is more than 0.3, and does not become supersonic. So a compressible flow solution is more appropriate. In compressible flow also FLUENT® solves the standard continuity and momentum equation, but the computation of scalar quantity and density is to be computed using ideal gas law. FLUENT® recommends SIMPLE algorithm for compressible flow. For the present simulation problem pressure inlet and pressure outlet boundary conditions are used. A well posed set of inlet and exit boundary conditions for this flow are:

For flow inlet plane - Inlet total pressure, inlet static pressure, inlet total temperature, turbulent Kinetic energy and turbulent dissipation rate were to be specified.

For flow exit plane - Exit static pressure, exit total temperature, turbulent kinetic energy and turbulent dissipation rate were to be specified.

The inlet total pressure and inlet static pressure are kept same as the experimental work of Samsher [1]. The temperature at the inlet is calculated from ideal gas equation, which is obtained by compressing pressure from atmosphere to the total pressure at the inlet. The atmospheric temperature is assumed to be constant at 27 °C, though in experiment it varied from 20 °C to 35 °C. As the variation in temperature is not very large the dynamic viscosity is assumed constant at 27 °C (Dynamic viscosity (μ) = 1.846 $\times 10^{-5}$ N.s/m^2). The pressure outlet value at exit is assigned as zero gauge pressure, as the exit is directly exposed to atmosphere.

FLUENT® requires specification of transported turbulence quantities at inlet and outlet, when flow enters a domain. The turbulent kinetic energy and specific dissipation

rate at the inlet and outlet are assumed uniform in the present case. The turbulence quantities can be specified in terms of turbulence intensity, turbulent viscosity ratio, hydraulic diameter, and turbulence length scale. The turbulence intensity, I is the ratio of the root mean square of the velocity fluctuations, u', to the mean flow velocity, u_{avg}. The turbulence intensity at the core of a fully developed duct flow can be estimated from the following formula derived from an empirical correlation for pipe flows:

$$I = \frac{u'}{u_{avg}} = 0.16(\mathrm{Re}_{D_H})^{-1/8} \quad (4.27)$$

The turbulence length scale l, is physical quantity related to the size of the large eddies that contain the energy in turbulent flows. In fully developed flows, l is restricted by the size of the duct, since the turbulent eddies cannot be larger than the duct. An approximate relationship between l and the physical size of the duct is as following:

$$l = 0.07L \quad (4.28)$$

where L is the relevant dimension of the duct. The factor of 0.07 is based on the maximum value of the mixing length in fully developed turbulent pipe flow, where L is the diameter of the pipe. In a channel of non-circular cross-section, L can be based on hydraulic diameter. In the present case, as the flow is assumed fully developed, the hydraulic diameter is specified as $L = D_H$. The turbulent kinetic energy is derived from the turbulent intensity I as following:

$$k = \frac{3}{2}(u_{avg} I)^2 \quad (4.29)$$

where u_{avg} is the mean flow velocity.

The turbulent dissipation rate ε can be calculated from the turbulence length scale l, by the following relationship:

$$\varepsilon = C_{\mu}^{3/4} \frac{k^{3/2}}{l} \quad (4.30)$$

where C_μ is empirical constant specified in the turbulence model (approximately 0.09). From the above relations the values of turbulent kinetic energy and turbulent dissipation rate are calculated for inlet and outlet and specified in boundary conditions at inlet and outlet.

Behera [2] used mass flow boundary conditions at inlet, where velocity is computed from the velocity head available at the inlet and this velocity is used to compute the fluxes of all relevant solution variables into the solution domain. After each iteration, the computed velocity is adjusted so that the correct mass flow value is maintained. There are two ways to specify the mass flow boundary conditions. The first is the mass flow rate and the second is to specify the mass flux. If a total mass flow rate is specified, it converts internally to a uniform mass flux by dividing the mass flow rate by the total inlet area normal to the specified flow direction.

In the present problem, the total pressure and static pressure at the inlet are available, so pressure inlet boundary conditions can be used. When mass flow inlet boundary conditions are used, the velocity is calculated from the pressure difference which is further used in calculating the mass, but in the pressure inlet boundary conditions, there is no need of such calculations as both total pressure and static pressure are directly available. For the blade surfaces, wall boundaries are assigned and the roughness values are assigned as per the solution requirement. And for the rest of bounded edges, wall boundary conditions are prescribed.

4.6.2 Operating conditions

Operating pressure affects the solution in different ways for different flow regimes. In a low Mach number compressible flow (like the present simulation), the overall pressure drop is small as compared to the absolute static pressure and can be significantly affected by numerical round off. To avoid the problem of round-off error, the operating pressure (generally a large pressure roughly equal to the average absolute pressure in the flow) is subtracted from the absolute pressure. The relation between the operating pressure, gauge pressure and absolute pressure is expressed as:

$P_{abs} = p_{op} + p_{gauge}$ (4.31)

The location of the operating pressure is equally important when the computational output is to be compared with experimental results. So the location of the operating pressure is to be identified where the absolute static pressure is known. In the present problem the pressure parameter at inlet is known.

The operating pressure is considered 101325 Pa at the inlet measurement point, at x = -0.165 m and y = 0 m

The measurement plane is at 7.5 % distance of chord distance as shown in Figure 4.7.

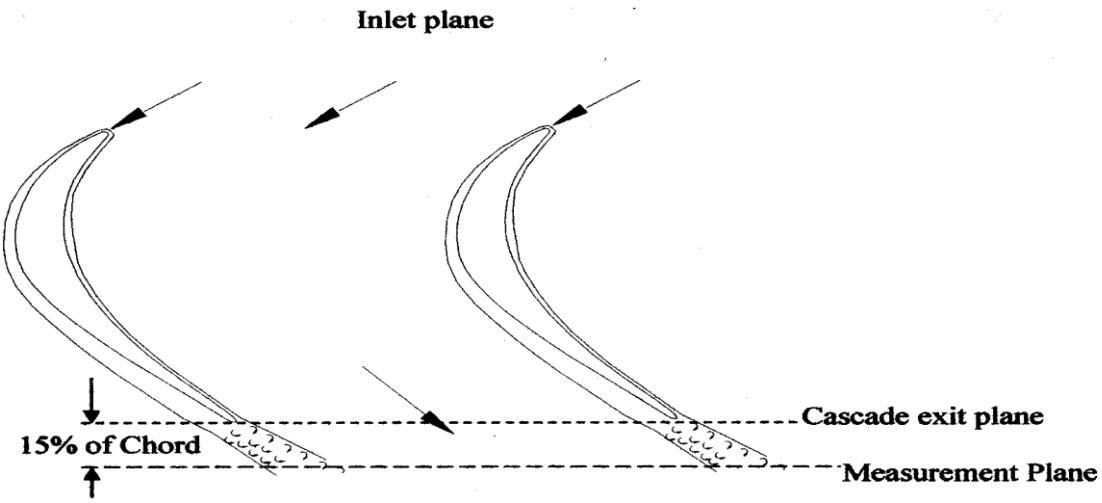

Figure 4.7 Measurement plane at 15% of the chord.

4.7 Profile loss calculations

The efficiency of cascade is expressed as Samsher [1]

$$\eta = \frac{h_1 - h_2}{h_1 - h_{2s}} = \frac{V_2^{\,2}}{V_{2s}^{\,2}} = \phi^2 \quad (4.32)$$

$$\eta = \frac{C_p(T_0 - T_2)}{C_p(T_0 - T_{2s})} = \frac{\left[1 - \frac{T_2}{T_0}\right]}{\left[1 - \frac{T_{2s}}{T_0}\right]} \tag{4.33}$$

Where C_p is the specific heat of air at constant temperature,T_0 is the temperature at inlet, T_2 is the actual temperature at exit and T_{2s} is the temperature at exit when expansion in the cascade is isentropic.

In the cascade, the total and static pressures at outlet, P_{02} and P_2 respectively and total pressure at inlet is P_{01}, are measured with yaw probe and total pressure probe. Therefore, in terms of the measured values, equation 4.33 can be written as:

$$\eta = \frac{\left[1 - \left[\frac{P_2}{P_{02}}\right]^{\frac{\gamma-1}{\gamma}}\right]}{\left[1 - \left[\frac{P_{2s}}{P_{01}}\right]^{\frac{\gamma-1}{\gamma}}\right]} \tag{4.34}$$

Where

$$\frac{P_2}{P_{02}} = \frac{P_2/P_{01}}{P_{02}/P_{01}} = \frac{P_2/P_{01}}{\frac{P_{01} - (P_{01} - P_{02})}{P_{01}}} = \frac{P_2/P_{01}}{1 - \left[\frac{P_{01} - P_{02}}{P_{01}}\right]}$$

$$= \frac{P_2/P_{01}}{1 - \left[\frac{P_{01} - P_{02}}{P_{01}}\right]\left[\frac{P_{01} - P_2}{P_{01} - P_2}\right]} \tag{4.35}$$

or

$$\frac{P_2}{P_{02}} = \frac{P_2/P_{01}}{1 - \left[\frac{P_{01} - P_{02}}{P_{01} - P_2}\right]\left[\frac{P_{01} - P_2}{P_{01}}\right]} = \frac{P_2/P_{01}}{1 - \left[\frac{P_{01} - P_{02}}{P_{01} - P_2}\right]\left[1 - \frac{P_2}{P_{01}}\right]} \tag{4.36}$$

Now substituting the value of P_2/P_{02} from equation in equation We have

$$\eta = \frac{1-\left[\frac{P_2/P_{01}}{1-\left[\frac{P_{01}-P_{02}}{P_{01}-P_2}\right]\left[1-\frac{P_2}{P_{01}}\right]}\right]^{\frac{\gamma-1}{\gamma}}}{\left[1-\left[\frac{P_{2s}}{P_{01}}\right]^{\frac{\gamma-1}{\gamma}}\right]}$$

Or

$$\eta = \frac{\left[1-\left[\frac{P_{01}-P_{02}}{P_{01}-P_2}\right]\left[1-\frac{P_2}{P_{01}}\right]\right]^{\frac{\gamma-1}{\gamma}}-\left[\frac{P_2}{P_{01}}\right]^{\frac{\gamma-1}{\gamma}}}{\left[1-\left[\frac{P_{2s}}{P_{01}}\right]^{\frac{\gamma-1}{\gamma}}\right]\left[1-\left[\frac{P_{01}-P_{02}}{P_{01}-P_2}\right]\left[1-\frac{P_2}{P_{01}}\right]\right]^{\frac{\gamma-1}{\gamma}}} \quad (4.37)$$

The profile loss coefficient ξ_y is calculated using the relation proposed by Dejc and Trojanovskij [expressed as

$$\xi_y = 1- \eta \quad (4.38)$$

Substituting the value of η in equation, we have

$$\xi_y = 1-\frac{\left[1-\left[\frac{P_{01}-P_{02}}{P_{01}-P_2}\right]\left[1-\frac{P_2}{P_{01}}\right]\right]^{\frac{\gamma-1}{\gamma}}-\left[\frac{P_2}{P_{01}}\right]^{\frac{\gamma-1}{\gamma}}}{\left[1-\left[\frac{P_{2s}}{P_{01}}\right]^{\frac{\gamma-1}{\gamma}}\right]\left[1-\left[\frac{P_{01}-P_{02}}{P_{01}-P_2}\right]\left[1-\frac{P_2}{P_{01}}\right]\right]^{\frac{\gamma-1}{\gamma}}} \quad (4.39)$$

On simplification the above equation and putting value of $P_2 = P_{2s}$ (as both points are on same pressure line), equation 3.38 is expressed as follow

$$\xi_y = \left[\frac{P_{2s}}{P_{01}}\right]^{\frac{\gamma-1}{\gamma}} \frac{1-\left[1-\left[\frac{P_{01}-P_{02}}{P_{01}-P_{2s}}\right]\left[1-\frac{P_{2s}}{P_{01}}\right]\right]^{\frac{\gamma-1}{\gamma}}}{\left[1-\left[\frac{P_{2s}}{P_{01}}\right]^{\frac{\gamma-1}{\gamma}}\right]\left[1-\left[\frac{P_{01}-P_{02}}{P_{01}-P_{2s}}\right]\left[1-\frac{P_{2s}}{P_{01}}\right]\right]^{\frac{\gamma-1}{\gamma}}} \quad (4.40)$$

The effect of change of pitch distance on the profile loss is shown in Figure

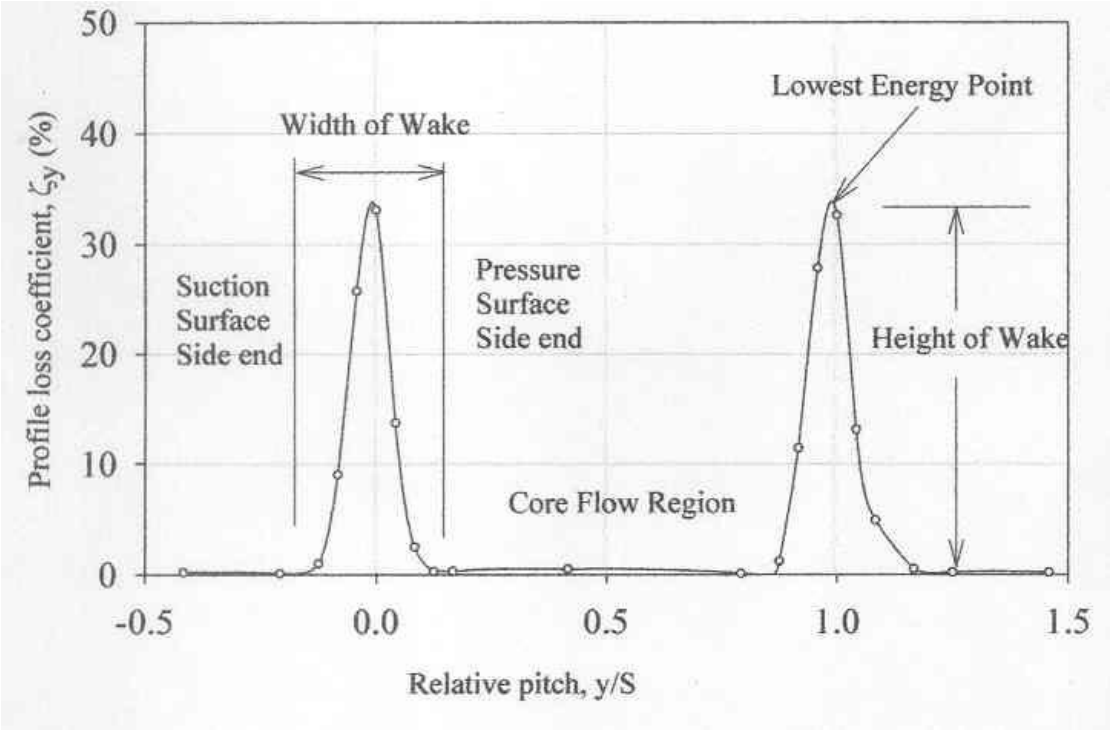

Figure 4.8 Profile loss coefficient versus relative pitch.

Where, P_{2s} is static pressure at outlet of cascade, P_{01} and P_{02} are the total pressures at the inlet and outlet of cascade respectively, γ is the ratio of specific heats for air.

To calculate a single value of energy loss coefficient, the mass average value of loss coefficient were calculated using the relation from.

$$\xi = \frac{\int_0^s \xi_y \rho V_a dy}{\int_0^s \rho V_a dy} \quad (4.41)$$

Where ξ is the mass average loss coefficient, V_a is the axial velocity, ρ is the density of air, S is the pitch distance and dy is the elemental length in pitch wise direction.

The non-dimensional zed parameter static pressure coefficient at a location on the blade surface is given as follows:-

$$C_p = \frac{P_i - P_{1s}}{\frac{1}{2}\rho V_1^{\,2}} \quad (4.42)$$

Where C_p is the static pressure coefficient, ρ is the density of air, P_i is the static pressure at the location on the blade, P_{1s} is static pressure at the inlet of cascade and V_1 is the velocity of air at inlet of cascade.

Chapter 5

RESULTS AND DISCUSSSION

5.1 Effect of Roughness applied over Different profiles on loss coefficient:

The roughness's of different levels have been applied over various locations of different profiles and the loss coefficient at exit of the cascade has been discussed here. Roughnesses of 0.5 mm and 1mm have been applied over pressure surface, suction surface and over both surfaces separately for all the three profiles.

The total pressure distribution for a typical case over the entire computation domain is shown in figure 5.1. The total pressure remains constant before the compressed fluid enters the cascade section. After entering the cascade section the total pressure reduces due to viscous drag over the cascade section and at the exit of the cascade the wakes are formed, where the total pressure drops significantly, however in the core flow region, the pressure drop is very less. At significant distance from the trailing edge the intermixing of the core flow and the wake takes place and the total pressure drops. Width of the wake depends on the pressure drop in the cascade section, higher is the pressure drop and larger is the width of the wake. The cascade has total 5 channels made with six blades. The two channel of either side have the effect of the side walls. Thus to see the effect of roughness over the blade only middle channel is considered. The shape of the wake shaded by extreme ends differ from middle one this can be minimised by modification of total board/ line at exit of the cascade.

The results shows the loss coefficient along the measuring plane. The height and width of the wake present the together represent the loss occurring due to roughness. The roughness increases viscous loss as well may cause separation of boundary layer. The trends of the results are very much similar to the experimental results of Samsher (2002).

5.2 Effect of change in roughness over profile 6030:

Initially roughness of 0.001 and 0.005 was applied over only pressure surface, i.e. suction surface remained smooth. The variation in loses coefficient are shown in fig 5.2 and 5.3. There is significant increase in loss coefficient. The wake height as well width of wake represent total energy loss due to roughness.

The effect of roughness over suction surface is shown in fig 5.4 and 5.5. The height of is almost unchanged but thickness of the wake is increased due to roughness indicating increase in total loss. Similar effect is also seen while roughness is put on both the surfaces and shown in fig 5.6 and 5.7.

5.3 Effect of roughness over profile 5530:

The effects of roughness over pressure, surface, suction surface, and over both the surfaces together for roughnesses levels of 0.001 and 0.005 m over both the surface are shown in fig 5.8, 5.9,5.10, 5.11, 5.12 and 3.13 respectively.

In this, it seems that total loss coefficient has some to negative value at middle of the channel.

It may be due to very high dynamic head at the centre due to thicker boundary layer over the blade caused by roughness. Result reveals that the loss coefficient increases with increase in roughness. The roughness over pressure is less detrimental than roughness over suction surface.

5.4 Roughness over profile 3525:

The figures 5.14, 5.15, 5.16, 5.17, 5.18, 5.19 shows the effect of roughness over pressure surface, suction surface and both surfaces together. The wakes of this profile are thicker compared to other two profiles. This indicates that intermixing of core flow with wake is more making the wake thicker and shorter also. Here, also the roughness over pressure surface is less detrimental than the same over suction surface.

5.5 Compression of Effect roughness across the profiles:

From the figures discussed above, it can be seen that the same roughness over reaction profiles (6030 and 5530) is more detrimental than impulse profile 3525.

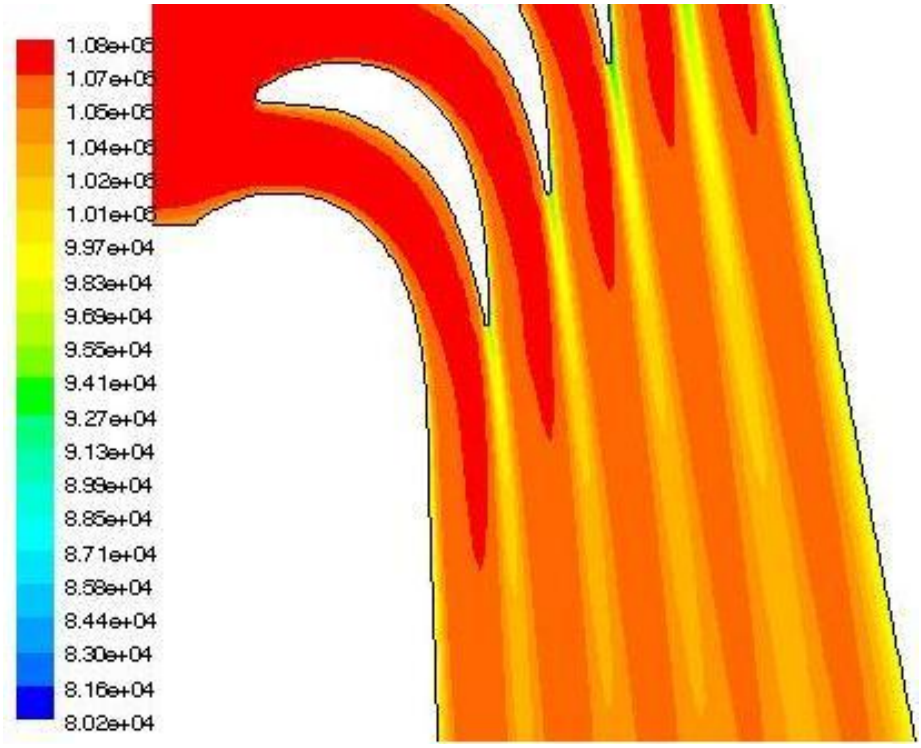

Figure 5.1 Total pressure distributions in wake region for smooth blade in Pa.

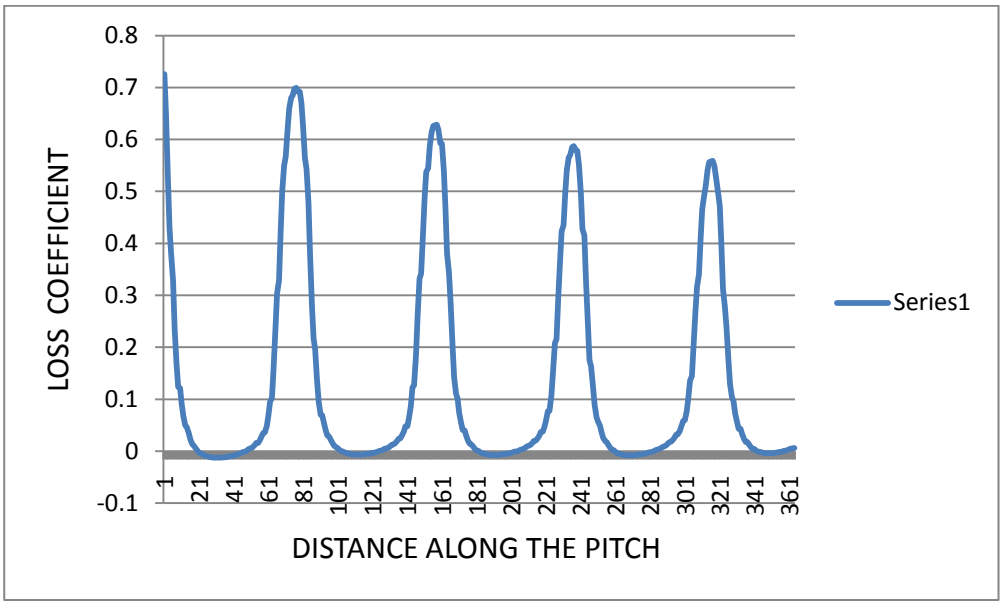

Figure: 5.2 Variation in loss coefficient for profile 6030 for roughness over Pressure surface only (ps 0.001. and ss 0.00)

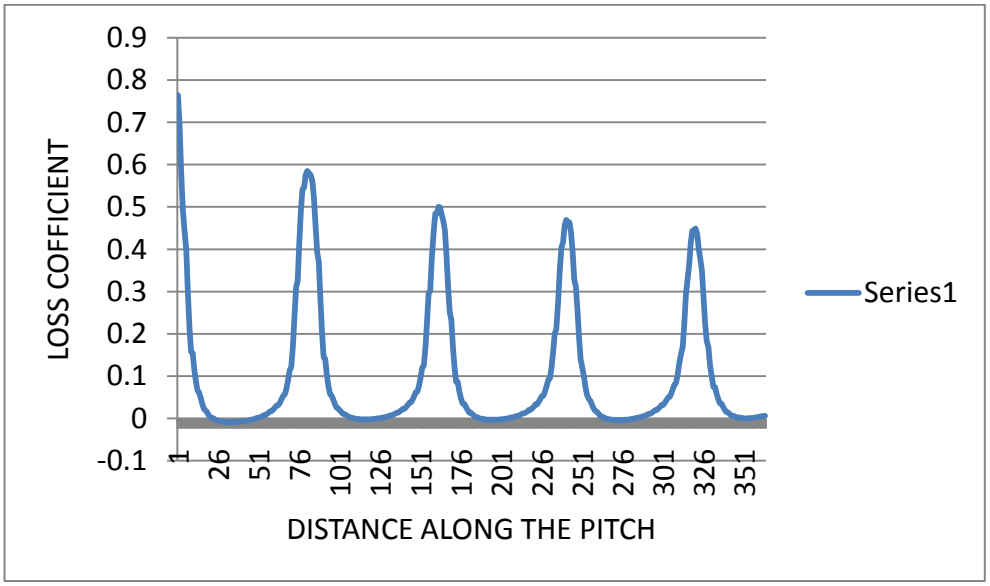

Figure 5.3 Variation in loss coefficient for profile 6030 for roughness over pressure surface only (ps 0.005 and ss 0.00)

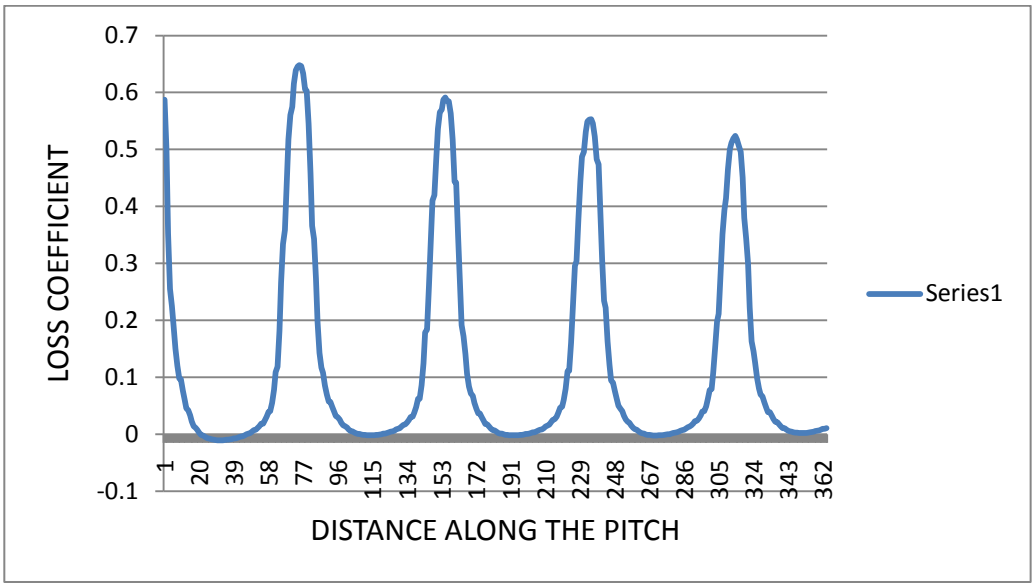

Figure: 5.4 Variation in loss Coefficient for profile 6030 for roughness over suction surface only (ps 0.005 and ss 0.00)

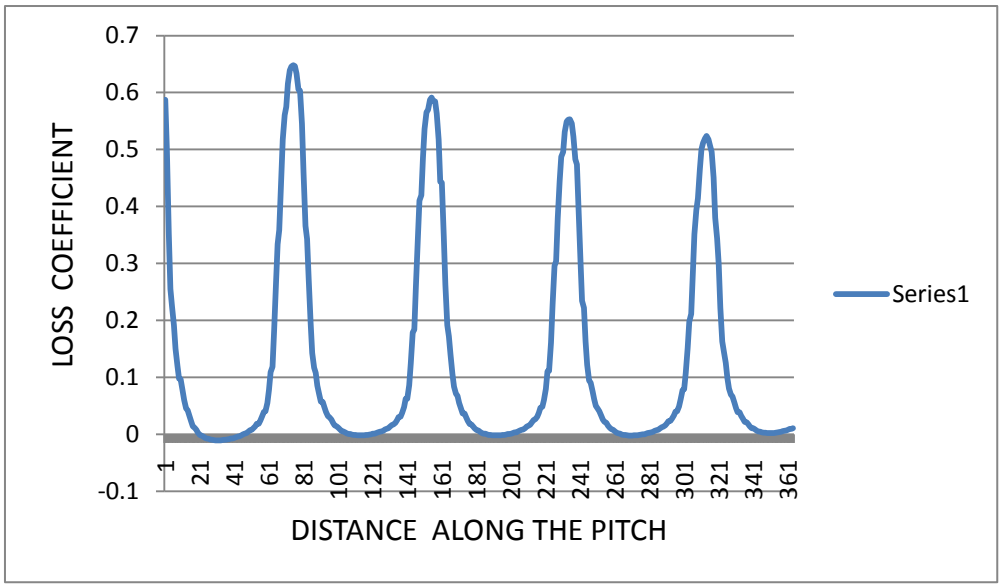

Figure 5.5 Variation in loss Coefficient for profile 6030 for roughness over suction surface Only (ps 0.00 and ss 0.001)

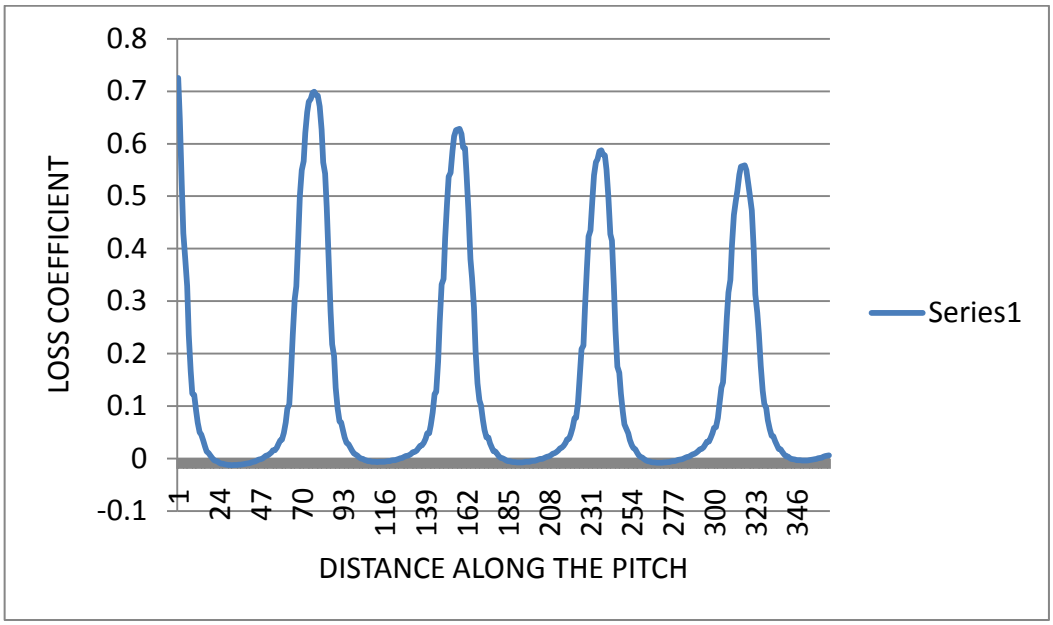

Figure: 5.6 Variation in loss Coefficient for profile 6030 for roughness over both Pressure surface and suction surface (ps 0.001 and ss 0.001)

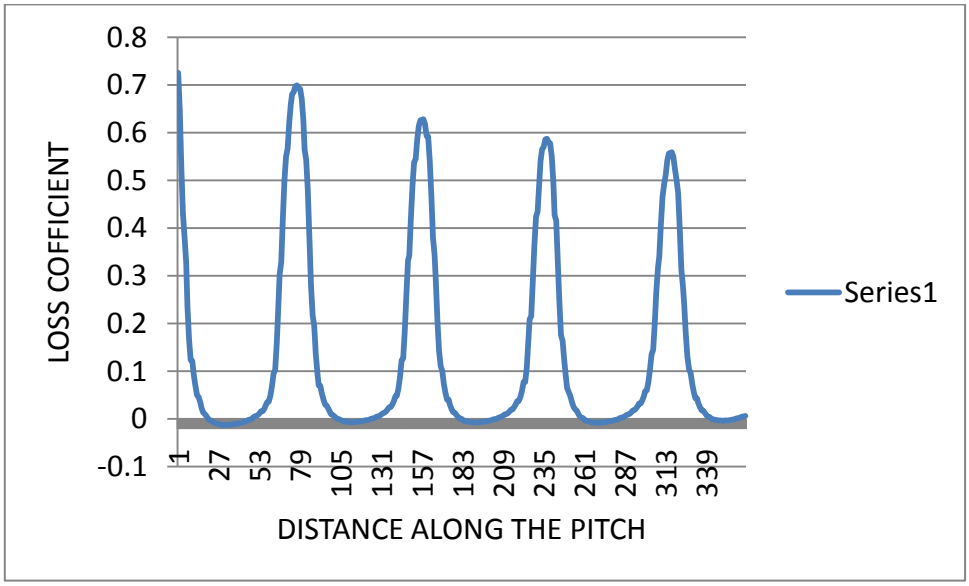

Figure: 5.7 Variation in loss coefficient for profile 6030 for roughness over both pressure surface and suction surface (ps 0.005 and ss 0.005)

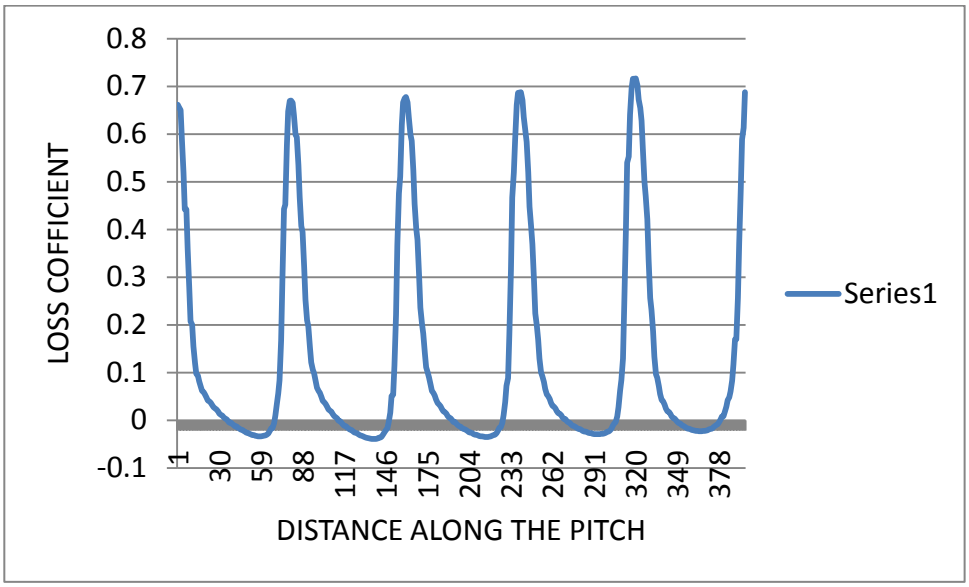

Figure:5.8 Variation in loss Coefficient for profile 5530 for roughness over Pressure surface only (ps 0.005 and ss 0.00)

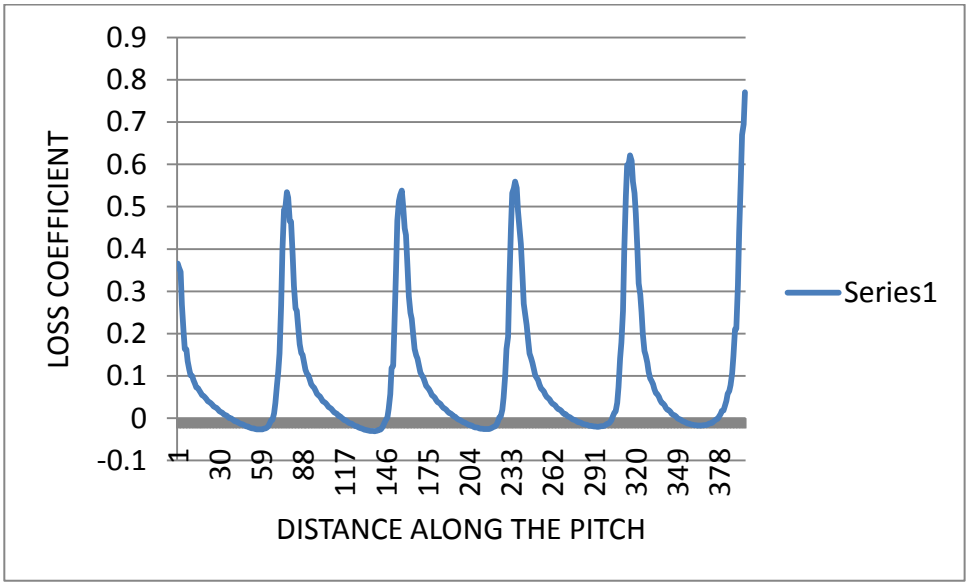

Figure: 5.9 Variation in loss coefficient for profile 5530 for roughness over pressure surface only (ps 0.001 and ss 0.00)

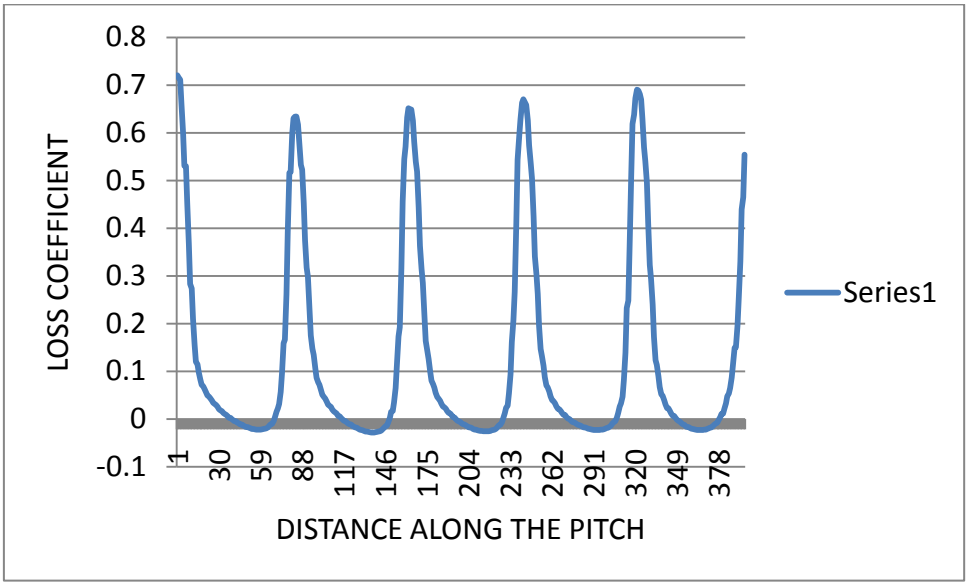

Figure: 5.10 Variation in loss coefficient for profile 5530 for roughness over suction surface only (ps 0.00 and ss 0.005)

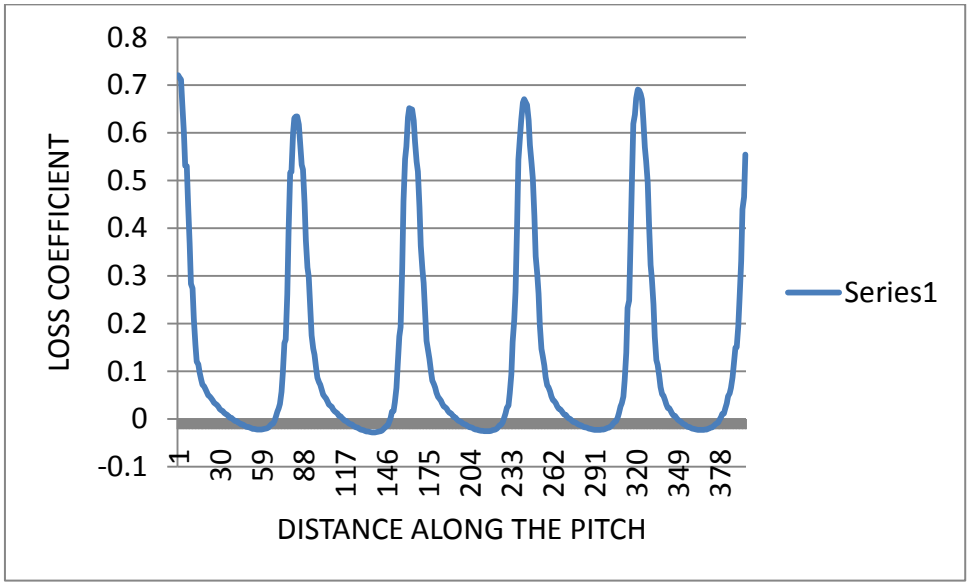

Figure: 5.11 Variation in loss Coefficient for profile 5530 for roughness over Suction surface only (ps 0.00 and ss 0.001)

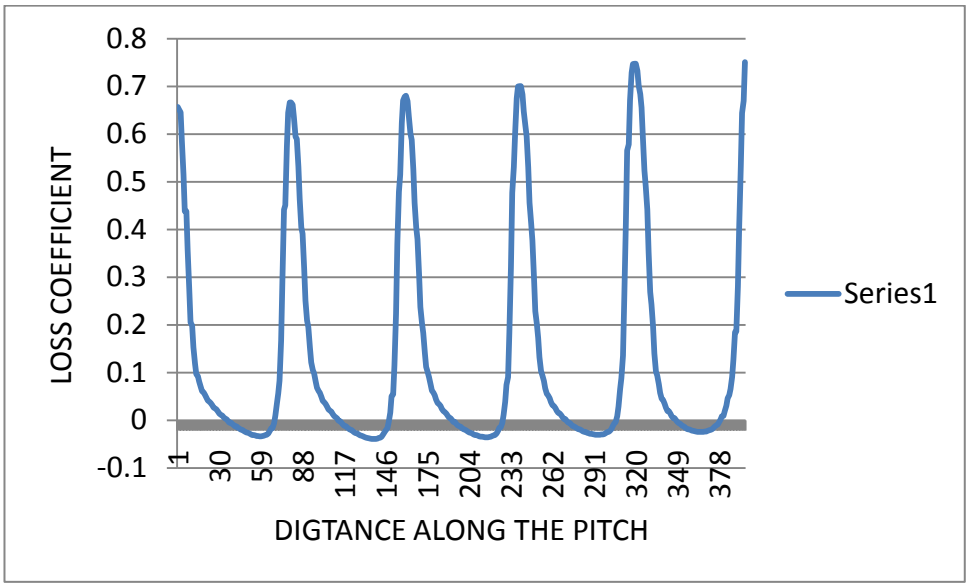

Figure: 5.12 Variation in loss Coefficient for profile 5530 for roughness over both pressure surface and suction surface(ps 0.005 and ss 0.005)

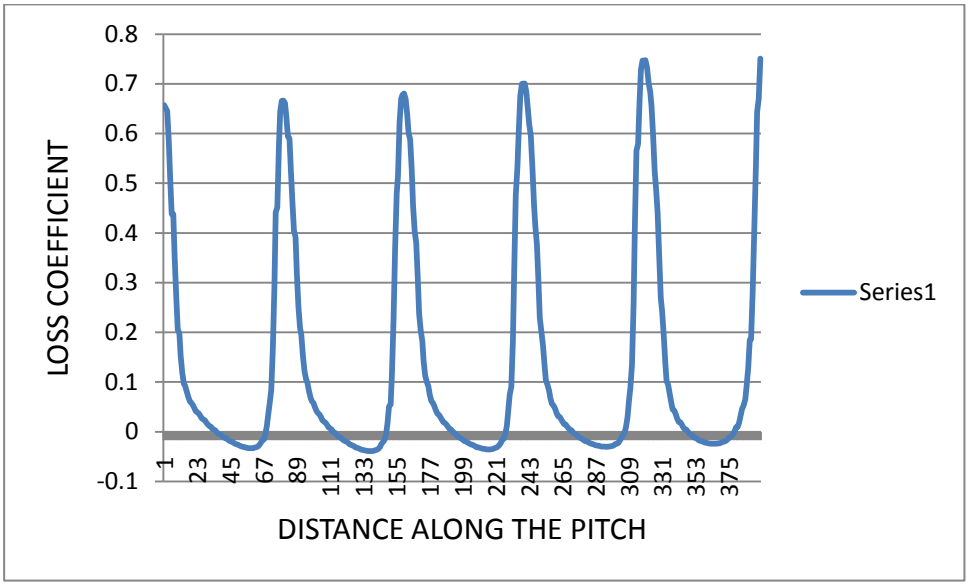

Figure: 5.13 Variation in loss Coefficient for profile 5530 for roughness over both pressure surface and suction surface (ps 0.001 and ss 0.001)

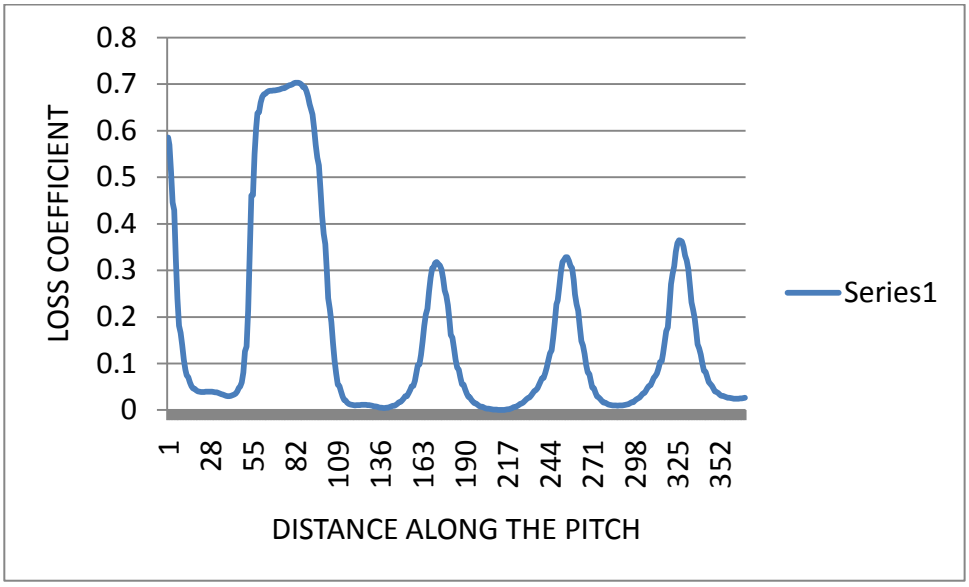

Figure: 5.14 Variation in loss Coefficient for profile 3525 for roughness over pressure surface only (ps 0.005 and ss 0.00)

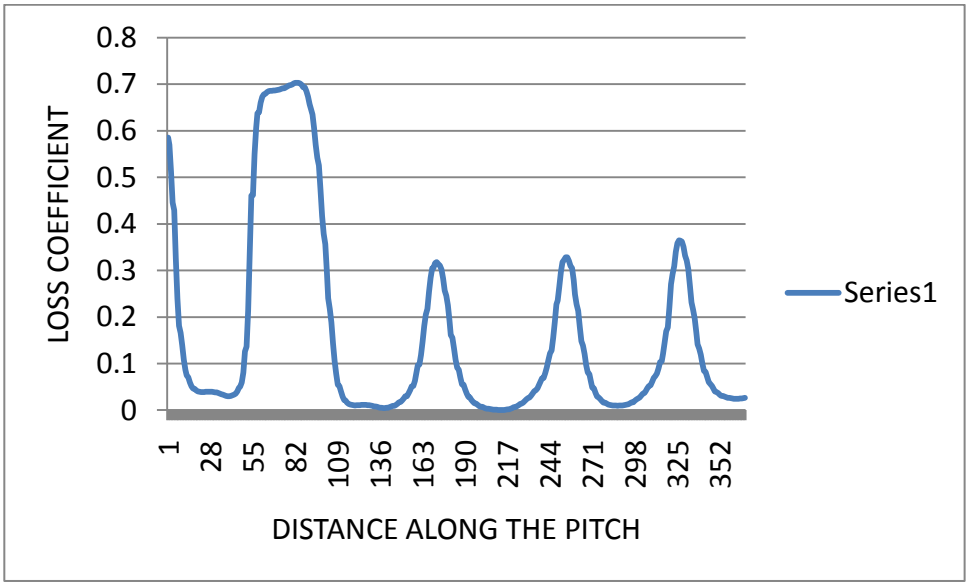

Figure: 5.15 Variation in loss Coefficient for profile 3525 for roughness over pressure surface only (ps 0.001 and ss 0.00)

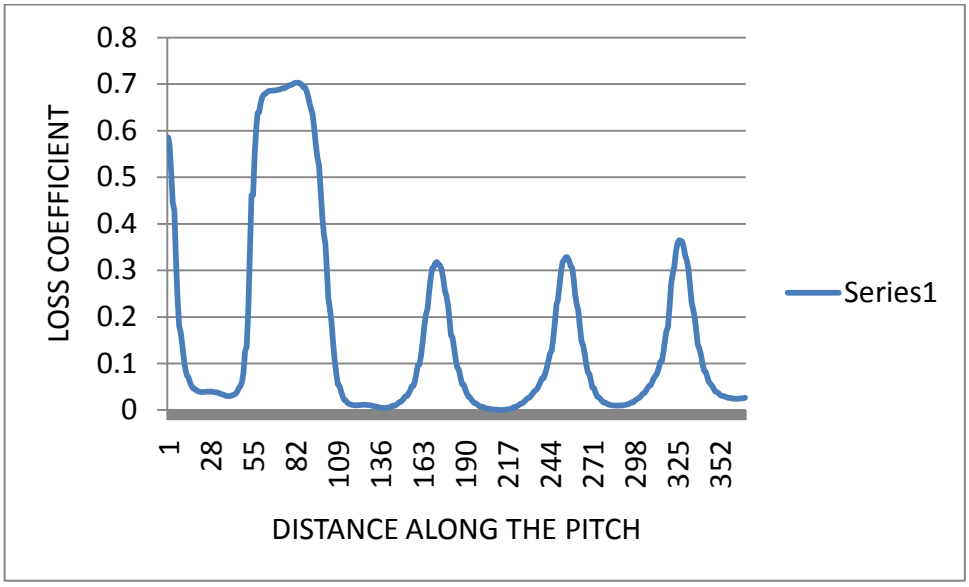

Figure: 5.16 Variation in loss Coefficient for profile 3525 for roughness over suction surface only (ps 0.00 and ss 0.005)

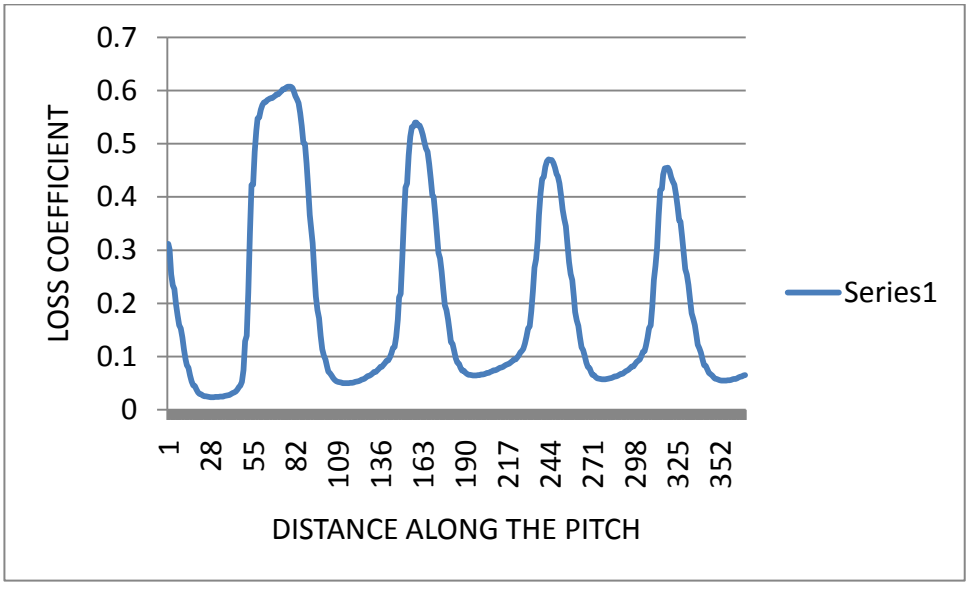

Figure: 5.17 Variation in loss Coefficient for profile 3525 for roughness over suction surface only (ps 0.00 and ss 0.001)

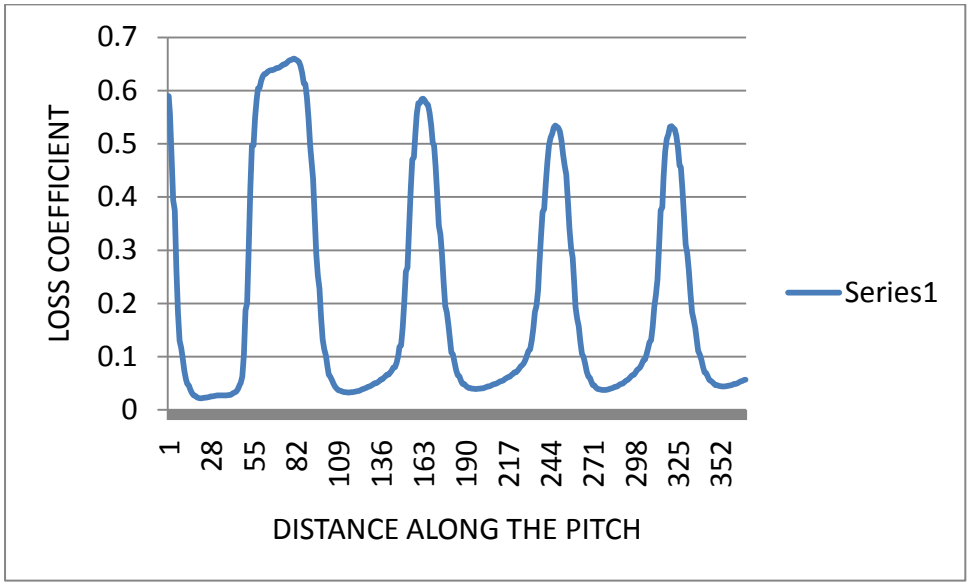

Figure: 5.18 Variation in loss Coefficient for profile 3525 for roughness over both pressure surface and suction surface(ps 0.005 and ss 0.005)

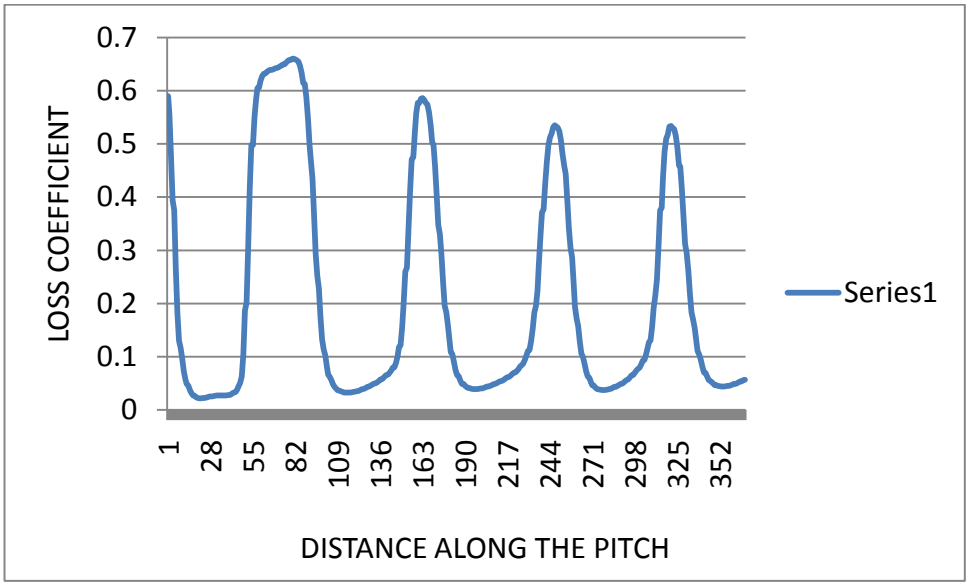

Figure:5.19 Variation in loss Coefficient for profile 3525 for roughness over both pressure surface and suction surface (ps 0.001 and ss 0.001)

Chapter 6

CONCLUSION

From the present study the following can be concluded

1. The roughness over the blade varies from stage to stage and also from blade hub to tip.

2. The loss affect increases with increase in roughness in each profile.

3. The roughness over pressure surface is more detrimental than the same over suction surface.

4. The roughness over reaction profiles (6030 and 5530) more detrimental than the same over impulse profile is 3525.

5. The roughness increases width and height of the wake.

Chapter 7

SCOPE FOR FUTUR WORK

During the present work, it has been observed that there are areas that require further investigations; some of these are given below.

1. The past experiment and present computational investigations were carried out only for the profile losses of the turbine blade cascade. Further work need to be carried out for end losses of the turbine blade cascade.
2. The experiments were done by applying extra layer of thickness on the blade profiles which simulate the effect of deposition on the turbine blades. The experimental and computational studies need to be done by removing a layer from the turbine blades on leading as well as trailing edge to simulate erosion phenomenon prevalent in the steam and gas turbines.
3. Experiment studies can be extended to study a wider range of profiles encountered in steam and gas turbines.
4. Change in the momentum thickness in the blade profile on the different level such as pressure surface and suction surface on the blade.

REFERENCES

1. Samsher, "Effect of blade surface roughness on profile loss at exit angle in a Rectilinear Stesm turbine cascade", Ph.D. Thesis, IIT Delhi, December 2002.
2. Bhera, L., K., "Study of turbine blade roughness and its performance", M.Tech. Thesis, IIT Delhi, May 2005.
3. Yi Li, "Aerodynamics and heat transfer predictions in a highly loaded turbine Blade". May 2007, 28, pp 932 – 937
4. Li Wei and Qiao Weiyang," Tip clearance flows in turbine cascades", November 2008, 21, pp 193 – 199.
5. Qiang Xiaoging and Wang Sangtao, "Aerodynamic design and analysis of Low Reaction axial Compressor stage", June 2008, 21, pp 1 – 7.
6. Song Woo Lee and Jin Jae Park, " Effect of incidence angle on end wall Convective Transport with in a high turning turbine rotor passage", September 2009, 52, pp 5922 – 5931.
7. Kim Jin Wook and Kim Tongbeum, "Effect of the leakage flow tangential Velocity In shrouded axial compressor cascades", December 2009, 14, pp 105 – 110.
8. Qi Lei and Liu Huoxing, "Upstream wake secondary flow interaction in the end Wall Region of high loaded turbines", June 2010, 39, pp 1575 – 1584.
9. Guo shaung and chen shaowen, " Effect of boundary layer suction on aerodynamic Performance in a high load compressor cascade", 2010, 23, pp 179 – 186.
10. I . A. Hamakhan and T. Korakianitis, " Aerodynamic performance effects of leading edge geometry in gas turbine blades", September 2010, 87, pp 1591 – 1601.
11. Seong Eun Lee and Song Woo Lee, " Tip leakage aerodynamics over stepped squealer in a turbine cascade", August 2011, 35, pp 135 – 145.

12. Awatef A . Hamed Widen Tabakoff, Richard B. Rivir, "Turbine blade surface deterioration by Erosion", Journal of turbomachinery, July 2005 vol. 127.

13. Hamed, A., Tabakoff, W., Rivir, R. B., Das, K., Arora, P., "Turbine blade surface deterioration by erosion", ASME J. Turbomach., July 2005, **127**, pp 445-452.

14. Hummel, F., Loetzerich, M., Cardamone, P., and Fottner, L., "Surface roughness effects on turbine blade Aerodynamics", ASME J. Turbo mach., July 2005, **127**, pp 453-461.

15. Zhang, Q., Goodro, M., and Ligrani, P., M., Trindade, R., Shreekanth, S., "Influence of surface roughness on the aerodynamic losses of a turbine vane", ASME Paper No. GT-2005-68832.

16. Zhang, Q., Ligrani, P., M., and Lee, S., W., "Determination of rough-surface skin friction coefficients from wake profile measurements", Experiments in Fluids **35**(2003) 627-635.

17. C.R.F. Azevedo and A. Sinatora, Erosion-Fatigue of steam turbine blades, Engineering Failure Analysis 16 (2009) 2290 – 2303.

18. B. S. Mann, Solid- particle erosion and protective layers for steam turbine balding, wear 224 (1999) 8 – 12.

19. J.W. Harpster, on condenser tube Corrosion and turbine blade copper deposition, 11th Southwest chemistry workshop, park city, Utah, august 13 – 15, 2002

20. Kang, S., H., Kang, Y., S., and Han, K., H., "Numerical study on blade roughness effect on the performance of turbo machines", IGTC 2003, Tokyo TS-033.

21. Yahya, S.,M., "Turbines, compressors and fans", Tata McGraw-Hill, New Delhi (2002).

22. Fluent 6.1 "User's Guide", Fluent Inc. 2003.

23. Budwing, R.S., "The boundary layer over turbine blade models with realistic rough Surfaces", University of Idaho, July 2002.

24. Ellering, C., P., "The combined effects of free stream turbulence, pressure gradient, and Surface roughness on the turbine aerodynamics", M.S. thesis, Air Force Institute of Technology, Wright Patterson Air Force Base, Ohio, March 2002.

APPENDIX -1

Coordinates of the profile 3525 of Samsher [1]

X	Y	X	Y	X	Y
0.40	0.37	40.39	24.81	37.78	11.45
0.30	0.34	41.48	24.01	35.46	12.43
0.20	0.34	42.42	23.25	34.11	12.89
0.06	0.38	43.39	22.29	32.86	13.24
-0.03	0.52	44.31	21.26	31.91	13.47
0.03	0.87	45.12	20.17	30.23	13.81
0.18	1.21	46.02	18.71	28.56	14.02
0.36	1.61	46.72	17.39	27.05	14.10
0.72	2.27	47.39	15.99	25.91	14.13
1.16	2.99	48.09	14.42	24.68	14.09
1.47	3.49	48.9	12.41	23.28	13.98
1.76	3.96	49.51	10.36	21.82	13.79
2.25	4.74	50.03	7.88	19.69	13.39
3.09	6.14	50.33	6.16	17.82	12.84
3.88	7.42	50.53	4.77	16.1	12.17
5.26	9.49	50.61	4.03	14.39	11.41
6.68	11.48	50.66	3.59	12.44	10.32
7.88	13.10	50.73	2.78	11.00	9.39
8.93	14.48	50.76	2.13	9.91	8.65
9.85	15.65	50.76	1.33	9.05	8.05
10.95	16.98	50.74	1.02	8.18	7.39
11.85	18.03	50.66	0.45	7.20	6.66
13.44	19.84	50.55	0.13	5.81	5.56
15.09	21.56	50.36	-0.03	4.57	4.40
17.03	23.28	50.26	-0.06	3.32	3.07
18.92	24.79	50.14	-0.06	2.70	2.30
20.62	25.85	49.89	0.03	1.93	1.47
21.88	26.44	49.57	0.32	1.71	1.23
22.77	26.85	49.11	0.86	1.44	0.96
24.16	27.36	48.82	1.24	0.99	0.61
25.85	27.76	48.52	1.65	0.69	0.44
27.04	27.95	48.3	1.96	0.40	0.37
27.96	28.06	48.12	2.21		
29.11	28.14	47.81	2.65		
30.14	28.14	47.16	3.55		

31.15	28.09	46.54	4.36
32.09	28.00	45.66	5.40
32.09	27.79	44.97	6.16
33.40	27.48	43.91	7.18
34.66	27.08	42.77	8.16
35.90	26.52	41.76	8.92
37.35	25.65	40.92	9.50
39.09	25.65	39.52	10.44

Coordinates of the profile 6030 Of Samsher [1]

x	y	x	y	x	y
0.17	2.29	49.90	0.86	5.93	3.77
0.18	2.37	50.00	0.67	4.98	2.98
0.22	2.55	50.06	0.54	4.25	2.36
0.42	3.38	50.06	0.42	3.40	1.62
0.67	4.19	50.02	0.28	2.76	1.07
1.23	5.67	49.97	0.24	2.40	0.76
1.71	6.79	49.94	0.23	2.24	0.62
2.41	8.14	49.91	0.22	1.79	0.23
2.83	8.88	49.86	0.21	1.41	-0.09
3.93	10.69	49.72	0.20	0.83	-0.19
4.98	12.01	49.52	0.29	0.56	-0.16
6.38	13.43	49.28	0.41	0.35	-0.09
7.15	14.13	49.09	0.53	0.21	0.01
8.32	15.04	48.80	0.71	-0.01	0.22
9.51	15.80	48.52	0.89	-0.07	0.66
10.88	16.55	48.04	1.21	0.01	1.44
12.68	17.34	47.43	1.60	0.09	1.87
14.16	17.79	46.50	2.18	0.17	2.29
19.70	18.54	43.69	3.88		
21.15	18.47	41.80	4.95		
22.78	18.28	39.99	5.93		
25.04	17.89	38.54	6.68		
27.29	17.19	36.82	7.51		
29.35	16.33	35.45	8.12		

30.28	15.92	34.05	8.67
32.09	15.02	31.98	9.42
34.41	13.69	29.72	10.00
36.75	12.12	27.63	10.31
38.82	10.60	26.63	10.41
40.07	9.62	25.37	10.50
41.96	8.07	24.12	10.52
43.82	6.45	22.44	10.47
46.00	4.49	20.99	10.35
47.35	3.26	18.50	10.00
48.23	2.47	16.58	9.55
48.66	2.07	14.99	9.04
48.93	1.83	13.93	8.68
49.11	1.66	11.48	7.67
49.28	1.49	9.21	6.26
49.69	1.09	6.94	4.58

Coordinate of the profile 5530 of Samsher [1]

x	y	x	y	x	y
0.02	0.55	26.07	14.49	32.19	8.07
0.04	0.69	27.14	13.98	30.72	8.61
0.09	1.10	27.92	13.59	29.92	8.87
0.11	1.23	28.37	13.36	27.89	9.49
0.16	1.52	29.30	12.88	26.50	9.85
0.23	1.83	30.38	12.29	25.06	10.15
0.33	2.23	31.76	11.52	24.48	10.26
0.46	2.74	32.51	11.09	23.87	10.37
0.74	3.66	33.09	10.74	21.59	10.69
1.08	4.57	34.10	10.15	20.58	10.76
1.47	5.50	35.57	9.25	19.53	10.77
1.73	6.07	37.64	7.91	19.27	10.77
2.15	6.88	38.81	7.13	17.79	10.70
2.44	7.40	40.44	6.03	17.04	10.63
2.83	8.04	41.10	5.59	16.54	10.57
3.49	9.02	42.31	4.78	15.80	10.48
3.93	9.61	43.29	4.12	13.92	10.09
4.56	10.38	44.27	3.48	13.30	9.91
5.15	11.05	45.90	2.41	12.69	9.70
6.14	12.04	46.78	1.85	12.12	9.48
6.97	12.74	47.21	1.57	11.52	9.24
7.76	13.34	47.74	1.23	10.70	8.90
8.71	14.02	48.80	0.54	10.06	8.61

9.23	14.36	49.20	0.27	9.00	8.07
9.97	14.79	49.69	-0.22	8.01	7.53
10.63	15.14	49.70	-0.42	6.78	6.72
11.29	15.44	49.61	-0.60	5.92	6.00
12.10	15.77	49.49	-0.64	5.58	5.70
12.56	15.94	49.16	-0.58	4.78	4.96
13.33	16.19	48.94	-0.51	3.77	3.86
14.20	16.43	48.22	-0.19	2.70	2.55
14.78	16.57	47.70	0.08	2.32	2.07
15.14	16.65	46.69	0.64	2.01	1.66
15.85	16.78	45.75	1.17	1.71	1.27
16.45	16.84	44.35	1.98	1.49	0.99
17.51	16.89	43.19	2.65	1.26	0.69
18.78	16.82	41.22	3.76	1.07	0.44
19.34	16.74	39.82	4.53	0.69	0.01
20.33	16.54	38.49	5.22	0.51	0.00
21.11	16.31	37.75	5.60	0.31	-0.01
21.79	16.10	36.91	6.02	0.20	0.08
22.63	15.84	35.52	6.68	0.01	0.30
23.46	15.57	34.18	7.27	0.02	0.55
24.42	15.20	32.95	7.78		